Average stress in a dilute suspension of rigid spheroids in a second-order fluid in a linear flow

Tanvi Mahendra Apte [1], Arezoo Ardekani [2], and Vivek Narsimhan [1,*]
[1]*Davidson School of Chemical Engineering, Purdue University, West Lafayette, Indiana 47907, USA*
[2]*School of Mechanical Engineering, Purdue University, West Lafayette, Indiana 47907, USA*

(Received 10 December 2024; accepted 3 April 2025; published 15 May 2025)

The microhydrodynamics of particle suspensions in polymeric fluids has a wide range of applications in industry and biology. To discern the dynamics of particles in such systems, it is important to analyze the stress response of the suspension to applied flow fields. While such investigations have been theoretically done for suspensions of rigid spheres in weakly viscoelastic fluids, the effect of nonsphericity of particles on the stress remains relatively unexplored. The interplay between the response of the polymeric fluid and the particle orientation yields rich physics. The viscoelastic torques make the particle inhabit a preferred orientation in a given flow, resulting in time-dependent stresses. In this paper, we determine the average extra stress in a dilute suspension of rigid, non-Brownian spheroids in a second-order fluid subject to shear and extensional flows. We perform this task by examining the flow around a single spheroid in the limit of small Weissenberg number ($\mathrm{Wi} \ll 1$) and perform an ensemble average of the stress tensor over all particle configurations. There are two contributions to the extra stress: one from the force dipole on the particles (stresslet) and another from the fluctuations in the velocity in the bulk fluid (fluid-induced particle stress), the latter of which does not arise in a zero Reynolds number Newtonian fluid. We present results for the $O(\phi\mathrm{Wi})$ corrections to the long-time effective shear viscosity, normal stress coefficients, and extensional viscosities in the suspension in shear, uniaxial extensional, and planar extensional flows, where ϕ is the particle volume fraction. To elucidate the effect of particle shape on the effective viscosity, we repeat this analysis for different aspect ratios (A_R) for prolate (needlelike) and oblate (disklike) spheroids.

DOI: 10.1103/PhysRevFluids.10.053302

I. INTRODUCTION

Suspensions—i.e., particles embedded in liquids—are common in our everyday lives, as they are found in pharmaceutical drugs, biological fluids, foods, paints, and coatings. Suspensions often flow differently than simple fluids like water and air, and thus, it is important to characterize their flow behavior to better engineer and process them. For example, the effective viscosity of a suspension is a key variable of interest in designing microfluidic devices since phenomena like separation and flow focusing [1,2] hinge on the knowledge of the effective viscosity of the suspending medium. Homogenization is a useful tool for finding the effective material properties of a suspension through ensemble averaging. This topic has been studied for years for the case when particles are embedded in a simple Newtonian fluid like water. However, when the particles are inside a complex fluid like a polymer solution (polyvinylpyrrolidone, polyacrylamide, polyisobutylene, etc.), little is understood

*Contact author: vnarsim@purdue.edu

on how to calculate the effective material properties. In this paper, we will address such topics and investigate the role of particle shape on the effective stress in polymeric suspensions.

For a Newtonian fluid like water, the stress is given by the well-known equation $\boldsymbol{\sigma} = -p\mathbf{I} + 2\mu\mathbf{E}$, where $\boldsymbol{\sigma}$ is the stress tensor, p is the pressure, μ is the viscosity, and $\mathbf{E}$ is the rate of strain tensor. The presence of particles in a fluid provides an additional resistance to flow and induces an extra stress in the suspension. One of the earliest attempts to quantify extra stress in a Newtonian suspension due to the presence of particles was made by Einstein [3]. He posed that, for very dilute suspensions (particle fraction $\phi < 0.05$) of rigid spheres in a Newtonian fluid, the effective viscosity is given by $\mu(1 + 2.5\phi)$, where μ is the zero-shear viscosity of the fluid. Einstein's work was extended to systems with nonspherical particles by Jeffery [4] following the investigations of Edwardes [5] and Oberbeck [6]. Authors of numerous other studies also built on Einstein's theories [7,8]; however, a rigorous formal mathematical treatment of the homogenization procedure was put forth by Batchelor [9]. In this theory, the extra stress in a suspension with rigid particles arises from the average force dipole acting on the particles. A force dipole is a system of equal and opposite forces separated by a distance. When the forces act along the line separating them, they give rise to a stresslet, and when the force acts perpendicular to the line, they give rise to a couplet. The stresslet tries to pull apart or push into the particle, whereas the couplet tends to rotate the particle in the clockwise or anticlockwise direction. By virtue of the its rigidity, the particle tries to resist these deforming forces acting on it and thereby induces a stress in the suspension. Thus, Batchelor [9] established a relationship between the macroscopic bulk stress and the microscopic particle-scale force dipoles.

This research opened up avenues for exploring the rheology of more complex systems which emulate more realistic situations as seen in nature by relaxing the assumptions made by Batchelor [9] one by one. To study the effect of higher concentrations on the effective viscosity, it is imperative to understand hydrodynamic interactions between particles [10–12]. Brady and Bossis [13] studied the variation of effective viscosity with particle volume fraction for concentrated suspension ($\phi \sim 0.1$) of spheres in a simple shear flow. Their analysis revealed that hydrodynamic forces promote clustering of particles and increase effective viscosity, whereas short-range interparticle repulsive forces tend to prevent clustering and contribute negatively to the effective viscosity. They also provided a scaling law relation for the size of clusters. Rheology of suspensions has also been studied for other types of flow like plane Poiseuille flow [14] and pressure-driven flows [15]. The shape of suspended particles also influences the dynamics of the suspension. In this context, rodlike particle suspensions [16–18] have received significant attention. Spheroidal particles have also been investigated recently in several studies [2,19–22].

Batchelor's [9] study was restricted to particles in Newtonian fluids. However, many suspensions that we encounter daily are polymeric fluids. Polymeric fluids display unique flow behavior. For example, polymeric solutions exhibit viscoelasticity, behaving like a solid for flow timescales smaller than the polymer relaxation time and like a liquid for flow timescales longer than the polymer relaxation time [23]. When a polymeric fluid is sheared, it also experiences normal stresses in the flow that are not seen in purely viscous fluids. These normal stresses arise due to stretching of polymers in the flow direction, which generate tension along streamlines [24]. Lastly, polymeric fluids exhibit shear thinning, which is the decrease in effective viscosity of a fluid with an increase in shear rate. So far, the effective stress response of particles embedded in polymeric fluids is at its infancy [25], even though such knowledge would be important in many industrial applications. Authors of recent studies have examined the effective stress of a dilute suspension of rigid spheres in weakly viscoelastic polymer fluids. Here, the effective viscosity of the suspension was determined as well as expressions for the normal stress coefficients [26–28]. However, the effect of nonspherical particle shapes (e.g., rods and disks) in such fluids has yet to be examined, even though in many applications like fracking, it is common to see rodlike [17] and disklike particles [29] in polymer solutions. Authors of some studies have also investigated the orientation behavior of active particles in suspensions [30]. We anticipate that the rheology of nonspherical particles in polymer solutions will be interesting for many reasons. First, normal stresses in the solution will no longer make a particle tumble in a simple shear flow but instead orient to a preferred direction [2,17,20,31,32]. The

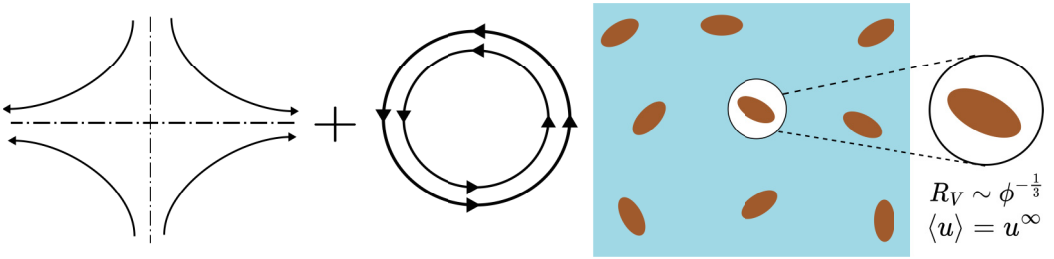

FIG. 1. Dilute suspension of spheroids in a second-order fluid under a linear flow field.

tendency of elongated particles to slowly assume a steady orientation will yield a time-dependent stress response. Secondly, the orientation of the particle can amplify the normal and extensional stresses seen in the solution compared with spheres, the effect to which has not been quantified.

This paper is structured in the following order. In Sec. II of this paper, we will discuss the problem setup (Sec. II A), followed by descriptions of background constitutive fluid (Sec. II B) and governing equations (Sec. II C). In Sec. III, we will perform homogenization techniques to determine expressions for the extra stress when particles are present in a viscoelastic fluid, and in Sec. IV, we will discuss numerical methods to evaluate this quantity. Section V summarizes the orientation behavior of prolate and oblate particles in viscoelastic fluids, and Sec. VI provides results for viscometric functions (e.g., shear viscosity, extensional viscosity, and normal stress coefficients) in shear, planar extensional, and uniaxial extensional flows. Section VII follows with conclusions.

II. PROBLEM FORMULATION

A. Setup

Figure 1 shows the problem setup. We consider a non-Brownian suspension of force-free, torque-free spheroids in a polymeric fluid under the action of an external linear flow. We would like to determine the average stress of the suspension. Since the suspension is considered dilute (volume fraction $\phi \ll 1$), one can examine the dynamics of a single particle and perform averaging over a representative volume $V = \phi^{-1} V_p$, where V_p is the particle volume. In Sec. III, we will discuss the averaging procedure in detail. Figure 2 shows the schematic of the individual particle dynamics. Here, we consider a particle in a background flow with an average rate of strain tensor $\langle \mathbf{E} \rangle$ and

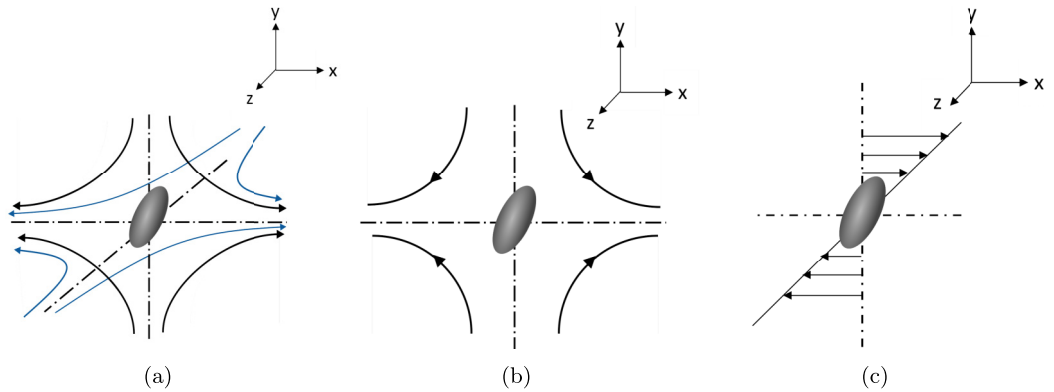

FIG. 2. Background flow fields for (a) uniaxial extension, (b) planar extension, and (c) shear flows.

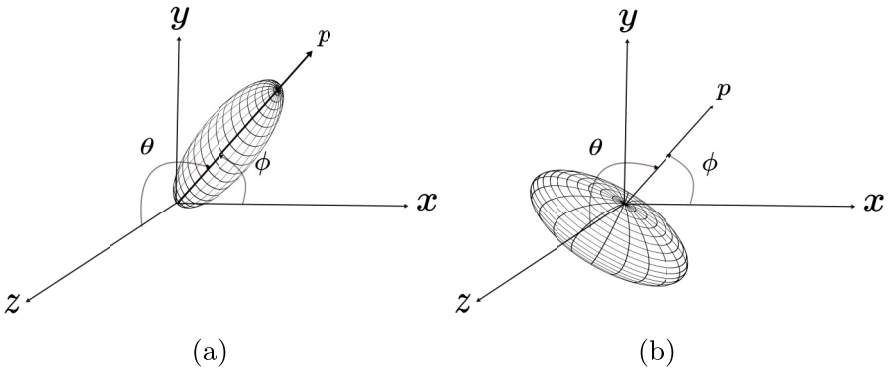

FIG. 3. Orientation angles for prolate and oblate geometries: θ is the polar angle defined between the z axis and the orientation vector, ϕ is the azimuthal angle defined between the x axis and the orientation vector.

average rate of rotation vector $\langle \mathbf{\Omega} \rangle$. The notation $\langle \dots \rangle$ represents an ensemble average;

$$\mathbf{u}^{\infty} = \langle \mathbf{E} \rangle \cdot \mathbf{x} + \langle \mathbf{\Omega} \rangle \times \mathbf{x}. \tag{1}$$

Three different linear flows are considered with characteristic shear rate/extension rate $\dot{\gamma}_c$:
(1) Shear flow: $u_x^{\infty} = \dot{\gamma}_c y$, $u_y^{\infty} = u_z^{\infty} = 0$:

$$\langle \mathbf{E} \rangle = \frac{\dot{\gamma}_c}{2} \begin{bmatrix} 0 & 1 & 0 \\ 1 & 0 & 0 \\ 0 & 0 & 0 \end{bmatrix}, \quad \langle \mathbf{\Omega} \rangle = -\frac{\dot{\gamma}_c}{2} \begin{bmatrix} 0 \\ 0 \\ 1 \end{bmatrix}; \tag{2}$$

(2) Planar extensional flow: $u_x^{\infty} = \dot{\gamma}_c x$, $u_y^{\infty} = -\dot{\gamma}_c y$, $u_z^{\infty} = 0$:

$$\langle \mathbf{E} \rangle = \dot{\gamma}_c \begin{bmatrix} 1 & 0 & 0 \\ 0 & -1 & 0 \\ 0 & 0 & 0 \end{bmatrix}, \quad \langle \mathbf{\Omega} \rangle = 0; \tag{3}$$

(3) Uniaxial extensional flow $u_x^{\infty} = \dot{\gamma}_c x$, $u_y^{\infty} = -\frac{1}{2}\dot{\gamma}_c y$, $u_z^{\infty} = -\frac{1}{2}\dot{\gamma}_c z$:

$$\langle \mathbf{E} \rangle = \frac{\dot{\gamma}_c}{2} \begin{bmatrix} 2 & 0 & 0 \\ 0 & -1 & 0 \\ 0 & 0 & -1 \end{bmatrix}, \quad \langle \mathbf{\Omega} \rangle = 0. \tag{4}$$

Figure 3 shows definitions of the spheroid geometry. The spheroid has semiaxis lengths a, b, and c, with $b = c$. For the prolate spheroid, a is the longest semiaxis ($a > b = c$), while for the oblate particle, a is the shortest semiaxis ($a < b = c$). The aspect ratio is defined as $A_R = a/b$ for a prolate spheroid and $A_R = b/a$ for the oblate spheroid, such that A_R is always $\geqslant 1$. The orientation vector $\mathbf{p}$ is defined by the direction along the a axis and is characterized by angles (θ, ϕ), where θ is the polar angle and ϕ is the azimuth angle. Here, θ is measured from the z axis to the orientation vector, and ϕ is measured from the x axis to the projection of the orientation vector on the x-y plane. The vector $\mathbf{p}$ is written as

$$\mathbf{p} = [\sin\theta \cos\phi, \sin\theta \sin\phi, \cos\theta]. \tag{5}$$

TABLE I. Examples of second-order fluids.

Composition	Molecular wt.	Viscosity	Relaxation time
Polyvinylpyrolidone (PVP) (3% by wt.) [2]	360 KDa	0.16 Pa s at 25 °C	2.3×10^{-3} s
Polyethylene oxide (PEO) (0.1% by wt.) [33,34]	4000 KDa	0.004 Pa s at 25 °C	0.02 s

B. Constitutive fluid model

Ordered fluid models are commonly used to describe small deviations from Newtonian behavior. In these models, the stress is expressed as a perturbation expansion about the known Newtonian stress equation in terms of the rate of strain [23]. These models are valid for small values of rate of strain—i.e., slow and nearly steady flow. An expansion up to second order leaves us with the second-order fluid model, the constitutive equation of which is below:

$$\boldsymbol{\sigma}^f = \boldsymbol{\sigma}^N + \boldsymbol{\sigma}^{\text{poly}}, \tag{6}$$

where $\boldsymbol{\sigma}^f$ is the fluid stress, broken into a Newtonian contribution $\boldsymbol{\sigma}^N$ and a non-Newtonian contribution $\boldsymbol{\sigma}^{\text{poly}}$:

$$\boldsymbol{\sigma}^N = 2\mu\mathbf{E} - p\mathbf{I}, \quad \boldsymbol{\sigma}^{\text{poly}} = -\psi_1 \overset{\nabla}{\mathbf{E}} + 4\psi_2 \mathbf{E}\cdot\mathbf{E}, \tag{7}$$

where

$$\mathbf{E} = \frac{\nabla\mathbf{u} + (\nabla\mathbf{u})^T}{2}, \tag{8}$$

$$\overset{\nabla}{\mathbf{E}} = \frac{D\mathbf{E}}{Dt} - (\nabla\mathbf{u})^T\cdot\mathbf{E} - \mathbf{E}\cdot\nabla\mathbf{u}. \tag{9}$$

In the above equation, $\mathbf{u}$ is the velocity field, p is the pressure, $\mathbf{E}$ is the rate of strain tensor, μ is the fluid viscosity, and ψ_1 and ψ_2 are the first and second normal stress coefficients, respectively. The term $\overset{\nabla}{\mathbf{E}}$ is called the upper-convected derivative, which is calculated in a frame of reference which translates and deforms with the fluid. This ensures that the constitutive equation is valid irrespective of the frame of reference in which it is evaluated.

The second-order fluid under a steady shear flow $u_x^\infty = \dot\gamma y$ predicts a shear stress $\sigma_{xy}^f = \mu\dot\gamma$ and normal stress differences $\sigma_{xx}^f - \sigma_{yy}^f = \psi_1\dot\gamma^2$, $\sigma_{yy}^f - \sigma_{zz}^f = \psi_2\dot\gamma^2$. In other words, the viscosity μ and normal stress coefficients $\{\psi_1, \psi_2\}$ do not exhibit shear thinning (i.e., a Boger fluid). The fluid has one relaxation time defined as $\lambda = \psi_1/(2\mu)$. At low strain rates, all constitutive models for polymeric fluids reduce to the second-order fluid model. An example of such is shown in Table I.

C. Governing equations

We will solve the steady flow around a spheroid in the polymeric fluid and use this information to compute the average stress in the suspension. Unless noted otherwise, all equations will be written in dimensionless form. We scale all lengths by the equivalent radius $R_c = (abc)^{1/3}$ of the spheroid, all times by the inverse characteristic shear rate $\dot\gamma_c^{-1}$, all velocities by $R_c\dot\gamma_c$, and all pressures and stresses by $\mu\dot\gamma_c$. The governing equations are the continuity and momentum equations:

$$\nabla\cdot\mathbf{u} = 0, \quad \nabla\cdot\boldsymbol{\sigma}^f = 0, \tag{10}$$

where the constitutive equation for the stress tensor is

$$\boldsymbol{\sigma}^f = \boldsymbol{\sigma}^N + \text{Wi}\boldsymbol{\sigma}^{\text{poly}}, \tag{11a}$$

$$\boldsymbol{\sigma}^N = 2\mathbf{E} - p\mathbf{I}, \quad \boldsymbol{\sigma}^{\text{poly}} = -2\overset{\nabla}{\mathbf{E}} + 8\alpha\mathbf{E}\cdot\mathbf{E}. \tag{11b}$$

In the above equation, there are two dimensionless numbers: a Weissenberg number Wi representing the ratio of polymer relaxation time to the flow timescale and a normal stress coefficient ratio α:

$$\mathrm{Wi} = \lambda\dot{\gamma}_c = \frac{\psi_1\dot{\gamma}_c}{2\mu}, \quad \alpha = \frac{\psi_2}{\psi_1}. \tag{12}$$

The equations are solved subject to the condition that the particle exhibits rigid body motion on its surface:

$$\mathbf{u} = \mathbf{U}^p + \boldsymbol{\Omega}^p \times \mathbf{x}, \quad \mathbf{x} \in S, \tag{13}$$

where $\mathbf{U}^p$ and $\boldsymbol{\Omega}^p$ are the translational and rotational velocities to be solved. The particle is force and torque free

$$\mathbf{F}^{\mathrm{ext}} = -\int (\boldsymbol{\sigma}^f \cdot \mathbf{n}) dS = 0,$$
$$\mathbf{T}^{\mathrm{ext}} = -\int \mathbf{x} \times (\boldsymbol{\sigma}^f \cdot \mathbf{n}) dS = 0, \tag{14}$$

where $\mathbf{n}$ is the normal vector pointing into the fluid phase. Lastly, far away from the particle, the velocity is the average background flow in the suspension. Since we are interested in dilute suspension rheology, one performs averaging over a characteristic volume $V = \phi^{-1}V_p$ that contains on average one particle. We thus enforce the boundary condition at a radius $r = R_V = \phi^{-1/3}$:

$$\mathbf{u} \to \mathbf{u}^\infty = \langle \mathbf{E} \rangle \cdot \mathbf{x} + \langle \boldsymbol{\Omega} \rangle \times \mathbf{x} \quad \text{at} \quad r = R_V = \phi^{-1/3}. \tag{15}$$

In general, one must enforce the boundary condition at this boundary rather than infinity to avoid divergences when volume averaging. However, if one is careful in the averaging procedure (as is done in this paper), one can apply the boundary condition at infinity and still obtain correct results (see Appendix 1).

Equations (10)–(15) are nonlinear and in general cannot be solved for arbitrary Weissenberg number Wi. Since the second-order fluid model is strictly valid only for $\mathrm{Wi} \ll 1$, we will solve the problem perturbatively. We expand the velocity and pressure fields as follows:

$$\mathbf{u} - \mathbf{u}^\infty = \mathbf{u}^{(0)} + \mathrm{Wi}\mathbf{u}^{(1)}, \quad p = p^{(0)} + \mathrm{Wi}p^{(1)}, \tag{16}$$

and perform a similar expansion for the translational and rotational velocities $\mathbf{U}^p = \mathbf{U}^{p,(0)} + \mathrm{Wi}\mathbf{U}^{p,(1)}$, $\boldsymbol{\Omega}^p = \boldsymbol{\Omega}^{p,(0)} + \mathrm{Wi}\boldsymbol{\Omega}^{p,(1)}$. We get the following equations at $O(1)$ and $O(\mathrm{Wi})$:

(1) ***O*(1) equations:** The $O(1)$ equations are the Stokes equations

$$\nabla^2\mathbf{u}^{(0)} - \nabla p^{(0)} = 0, \quad \nabla \cdot \mathbf{u}^{(0)} = 0, \tag{17}$$

subject to the conditions that the particle is force and torque free, the disturbance field is zero at the far-field boundary, and the disturbance field equal to $\mathbf{u}^{(0)} = \mathbf{U}^{p,(0)} + (\boldsymbol{\Omega}^{p,(0)} - \langle \boldsymbol{\Omega} \rangle) \times \mathbf{x} - \langle \mathbf{E} \rangle \cdot \mathbf{x}$ on the particle surface. The solution to this problem is well known (see Ref. [35]).

(2) ***O*(Wi) equations:** At $O(\mathrm{Wi})$, the equations are the Stokes equations with an inhomogeneous body force

$$\nabla^2\mathbf{u}^{(1)} - \nabla p^{(1)} = -\nabla \cdot \boldsymbol{\sigma}^{\mathrm{poly},D}, \quad \nabla \cdot \mathbf{u}^{(1)} = 0, \tag{18}$$

where $\boldsymbol{\sigma}^{\mathrm{poly},D} = \boldsymbol{\sigma}^{\mathrm{poly}}(\mathbf{u}^{(0)} + \mathbf{u}^\infty) - \boldsymbol{\sigma}^{\mathrm{poly}}(\mathbf{u}^\infty)$ is the $O(1)$ disturbance field for the polymeric stress—i.e., the polymeric stress evaluated at $\mathbf{u}^{(0)} + \mathbf{u}^\infty$ minus the quantity evaluated at $\mathbf{u}^\infty$. The above equation is subject to the conditions that the particle is force and torque free, the velocity decays to zero at the far-field surface, and the velocity is equal to $\mathbf{u}^{(1)} = \mathbf{U}^{p,(1)} + \boldsymbol{\Omega}^{p,(1)} \times \mathbf{x}$ on the particle surface.

In the next section, we will show that, to compute the average stress to $O(\mathrm{Wi})$, we do not need the full solution to the $O(\mathrm{Wi})$ velocity field. We need the $O(1)$ velocity field and the $O(\mathrm{Wi})$ contributions to translational velocity $\mathbf{U}^p$, rotational velocity $\boldsymbol{\Omega}^p$, and particle stresslet $\mathbf{S}^p$. The latter contributions

can be obtained from the $O(1)$ velocity fields using the reciprocal theorem. Details are provided in the next section.

III. HOMOGENIZATION

We are interested in determining the macroscopic average stress at any point in the suspension. The macroscopic stress can be related to the microscopic quantities by performing an ensemble average, that is, an average over all possible particle configurations. We will first write an expression for the ensemble average of the stress in terms of average and fluctuating components of the velocity field. We will then evaluate the expressions by replacing the ensemble averages with volume averages. In the following derivations, we will use index notation (i.e., Einstein notation) for convenience.

The total stress is composed of the fluid stress outside the particle and the particle stress inside the particle. Let χ be an indicator function

$$\chi = \begin{cases} 1, & \text{inside particle,} \\ 0, & \text{outside particle.} \end{cases} \tag{19}$$

In a suspension, the average stress is

$$\langle \sigma_{ij} \rangle = \left\langle (1-\chi)\sigma_{ij}^{f}(\mathbf{u}, \nabla\mathbf{u}) \right\rangle + \left\langle \chi \sigma_{ij}^{p}(\mathbf{u}, \nabla\mathbf{u}) \right\rangle = \left\langle \sigma_{ij}^{f}(\mathbf{u}, \nabla\mathbf{u}) \right\rangle + \left\langle \chi \sigma_{ij}^{p}(\mathbf{u}, \nabla\mathbf{u}) \right\rangle, \tag{20}$$

where $\sigma_{ij}^{f}(\mathbf{u}, \nabla\mathbf{u})$ is the stress in the fluid evaluated at $(\mathbf{u}, \nabla\mathbf{u})$ and $\sigma_{ij}^{p}(\mathbf{u}, \nabla\mathbf{u})$ is the stress in the particle evaluated at $(\mathbf{u}, \nabla\mathbf{u})$, and $\langle \dots \rangle$ represents an ensemble average. In the above equations, we make explicit that the fluid and particle stress fields are functions of the velocity $\mathbf{u}$ and velocity gradient $\nabla\mathbf{u}$ in the suspension. In going from the first to the second equality, we note that fluid stress $\sigma_{ij}^{f} = 0$ in the particle phase since the rate of strain is zero in a rigid particle.

Now we are interested in the extra stress in the suspension, which is the average stress minus the stress when the particles are absent. When particles are absent, the stress field everywhere is $\sigma_{ij}^{f}(\langle\mathbf{u}\rangle, \langle\nabla\mathbf{u}\rangle)$—i.e., the fluid stress evaluated at the mean velocity fields. Thus, the expression for the average extra stress in the suspension is

$$\left\langle \sigma_{ij}^{\text{ex}} \right\rangle = \left\langle \sigma_{ij}^{\text{fluct}} \right\rangle + \left\langle \chi \sigma_{ij}^{p} \right\rangle, \tag{21}$$

where

$$\left\langle \sigma_{ij}^{\text{fluct}} \right\rangle = \left\langle \sigma_{ij}^{f}(\mathbf{u}, \nabla\mathbf{u}) \right\rangle - \sigma_{ij}^{f}(\langle\mathbf{u}\rangle, \langle\nabla\mathbf{u}\rangle). \tag{22}$$

There are two contributions to the extra stress. There is a contribution from the particle phase called the extra particle stress $\langle \chi \sigma_{ij}^{p} \rangle$ and a term $\langle \sigma_{ij}^{\text{fluct}} \rangle$ arising from the fluctuations in the velocity field in the fluid, called the *fluctuating extra stress* or the *fluid-induced particle stress*. In a Newtonian fluid, the latter stress is zero since the fluid stress in linear in the velocity gradient, and thus, the right-hand side in Eq. (22) vanishes. However, when the fluid stress is nonlinear, fluctuations in the velocity field can give rise to a nonzero $\langle \sigma_{ij}^{\text{fluct}} \rangle$, analogous to a Reynolds stress in turbulence. The next subsections show expressions for both of these terms.

A. Fluctuating extra stress $\langle \boldsymbol{\sigma}_{ij}^{\text{fluct}} \rangle$

In a second-order fluid under a steady flow, the expression for the dimensionless fluid stress is

$$\sigma_{ij}^{f}(\mathbf{u}, \nabla\mathbf{u}) = 2E_{ij} - p\delta_{ij} - 2\text{Wi}\left(u_k \frac{\partial E_{ij}}{\partial x_k} - \frac{\partial u_j}{\partial x_k} E_{ik} - \frac{\partial u_i}{\partial x_k} E_{jk} \right) + 8\alpha \text{Wi} E_{ik} E_{kj}. \tag{23}$$

Evaluating the ensemble average of this stress gives

$$\left\langle \sigma_{ij}^{f}(\mathbf{u}, \nabla\mathbf{u}) \right\rangle = 2\mu\langle E_{ij}\rangle - \langle p\rangle\delta_{ij} - 2\mathrm{Wi}\left(\left\langle u_k \frac{\partial E_{ij}}{\partial x_k}\right\rangle - \left\langle \frac{\partial u_j}{\partial x_k} E_{ik}\right\rangle - \left\langle \frac{\partial u_i}{\partial x_k} E_{jk}\right\rangle\right) + 8\alpha\mathrm{Wi}\langle E_{ik}E_{kj}\rangle. \tag{24}$$

Similarly, evaluating the stress at the average velocity field yields

$$\sigma_{ij}^{f}(\langle\mathbf{u}\rangle, \langle\nabla\mathbf{u}\rangle) = 2\mu\langle E_{ij}\rangle - \langle p\rangle\delta_{ij} - 2\mathrm{Wi}\left(\langle u_k\rangle\left\langle \frac{\partial E_{ij}}{\partial x_k}\right\rangle - \left\langle \frac{\partial u_j}{\partial x_k}\right\rangle\langle E_{ik}\rangle - \left\langle \frac{\partial u_i}{\partial x_k}\right\rangle\langle E_{jk}\rangle\right) + 8\alpha\mathrm{Wi}\langle E_{ik}\rangle\langle E_{kj}\rangle. \tag{25}$$

We now subtract these two quantities to obtain the fluctuating stress $\langle\sigma_{ij}^{\mathrm{fluct}}\rangle$. The rate of strain can be written as the average rate of strain, i.e., the rate of strain of the background flow field, plus the fluctuating component that arises due to the particle:

$$E_{ij} = \langle E_{ij}\rangle + E'_{ij}, \tag{26}$$

where $\langle E_{ij}\rangle$ is the average rate of strain and E'_{ij} is the fluctuating component—i.e., $\langle E'_{ij}\rangle = 0$. Similarly, the velocity gradient can also be written as

$$\frac{\partial u_i}{\partial x_j} = \left\langle \frac{\partial u_i}{\partial x_j}\right\rangle + \frac{\partial u'_i}{\partial x_j}. \tag{27}$$

Subtracting Eq. (25) from Eq. (24) yields

$$\left\langle \sigma_{ij}^{\mathrm{fluct}}\right\rangle = -2\mathrm{Wi}\left(\left\langle u'_k \frac{\partial E'_{ij}}{\partial x_k}\right\rangle - \left\langle \frac{\partial u_j{}'}{\partial x_k} E'_{ik}\right\rangle - \left\langle \frac{\partial u_i{}'}{\partial x_k} E'_{jk}\right\rangle\right) + 8\alpha\mathrm{Wi}\langle E'_{ik}E'_{kj}\rangle. \tag{28}$$

The fluctuating extra stress is expressed as a function of the average of velocity fluctuations, like the Reynolds stress in turbulence.

We will now convert the ensemble average to a volume average. We average over a characteristic volume $V = \phi^{-1}V_p$, where V_p is the particle volume, since this volume contains on average one particle. Thus, the average of any quantity is

$$\langle f\rangle = \frac{1}{V}\int f dV = \frac{\phi}{V_p}\int_V f dV. \tag{29}$$

One can show that the first term in Eq. (28) is zero—i.e., $\langle u'_k \frac{\partial E'_{ij}}{\partial x_k}\rangle = 0$—due to the divergence theorem and the decay of the fluctuating velocity fields (see Appendix 2). Thus, the fluctuating stress is

$$\left\langle \sigma_{ij}^{\mathrm{fluct}}\right\rangle = 2\mathrm{Wi}\left(\left\langle \frac{\partial u_j{}'}{\partial x_k} E'_{ik}\right\rangle + \left\langle \frac{\partial u_i{}'}{\partial x_k} E'_{jk}\right\rangle\right) + 8\alpha\mathrm{Wi}\langle E'_{ik}E'_{kj}\rangle. \tag{30}$$

We now simplify the above expression further. We will break the averages into integrals over the particle phase and the fluid phase:

$$\langle f\rangle = \langle \chi f\rangle + \langle (1-\chi) f\rangle, \tag{31a}$$

$$\langle \chi f\rangle = \frac{\phi}{V_p}\int_{V_p} f dV, \quad \langle (1-\chi) f\rangle = \frac{\phi}{V_p}\int_{V_f} f dV. \tag{31b}$$

In the particle phase, the particle undergoes a rigid body motion with rotation rate $\mathbf{\Omega}^p$. Thus, the velocity gradient is $\frac{\partial u_i}{\partial x_j} = \epsilon_{ikj}\Omega_k^p$. Subtracting the average velocity gradient tensor $\langle \frac{\partial u_i}{\partial x_j}\rangle = \langle E_{ij}\rangle + \epsilon_{ikj}\langle \Omega_k\rangle$ from this quantity gives the fluctuating component

$$\frac{\partial u_i'}{\partial x_j} = \frac{\partial u_i}{\partial x_j} - \left\langle \frac{\partial u_i}{\partial x_j}\right\rangle = -\langle E_{ij}\rangle + \epsilon_{ikj}\left(\Omega_k^p - \langle \Omega_k\rangle\right),$$

$$E_{ij}' = -\langle E_{ij}\rangle, \quad \text{in particle.}$$

Substituting these expressions into Eq. (30) gives the particle phase contribution to the fluctuating stress

$$\left\langle \chi \sigma_{ij}^{\text{fluct}}\right\rangle = 2\phi \text{Wi}\left[(2+4\alpha)\langle E_{ik}\rangle\langle E_{kj}\rangle + \epsilon_{ikm}\langle E_{kj}\rangle\left\langle \Omega_m^p - \Omega_m\right\rangle + \epsilon_{jkm}\langle E_{ki}\rangle\left\langle \Omega_m^p - \Omega_m\right\rangle\right]. \tag{32}$$

If one wants to obtain this expression to $O(\text{Wi})$, it is sufficient to evaluate the average particle rotation rate relative to background flow $\langle \mathbf{\Omega}^p - \mathbf{\Omega}\rangle$ to the leading order. One can use the relationship $\langle \Omega^p - \Omega\rangle_m = M_{mkj}^{\Omega E}\langle E_{kj}\rangle$ for a force-free, torque-free particle, where $M_{mkj}^{\Omega E}$ is the Stokes flow mobility tensor, and plug it into the above equation.

To evaluate the fluid phase contribution to the fluctuating stress—i.e., $\langle (1-\chi)\sigma_{ij}^{\text{fluct}}\rangle$—we evaluate the averages in Eq. (30) using integrals over the fluid phase. This yields

$$\left\langle (1-\chi)\sigma_{ij}^{\text{fluct}}\right\rangle = \frac{2\text{Wi}\phi}{V_p}\int_{V_f}\left(\frac{\partial u_j'}{\partial x_k}E_{ik}' + \frac{\partial u_i'}{\partial x_k}E_{jk}' + 4\alpha E_{ik}'E_{kj}'\right)dV. \tag{33}$$

If one wants to obtain dilute suspension rheology—i.e., evaluate the extra stress to $O(\phi)$—the fluctuating velocity field u_i' is simply the disturbance field around a single particle. Thus, it suffices to use the leading-order disturbance velocity field $\mathbf{u}^{(0)}$ in Sec. II C to get the $O(\phi\text{Wi})$ correction to the average stress. One has to solve the disturbance field $\mathbf{u}^{(0)}$ in the finite control volume $V = \phi^{-1}V_p$ and then evaluate the above integral over the fluid region of the control volume. However, in Appendix 1, we demonstrate that correct results can be obtained by solving the disturbance field in an unbounded fluid (i.e., let $V \to \infty$) and evaluating the integral in Eq. (25) over the unbounded domain.

B. Particle extra stress $\langle \chi\sigma_{ij}^p\rangle$

To determine the particle extra stress $\langle \chi\sigma_{ij}^p\rangle$, we will replace the ensemble average with a volume average. We perform volume averaging over a characteristic volume $V = \phi^{-1}V_p$, which yields

$$\left\langle \chi\sigma_{ij}^p\right\rangle = \frac{1}{V}\int_{V_p}\sigma_{ij}^p\, dV = \frac{\phi}{V_p}\int_{V_p}\sigma_{ij}^p\, dV. \tag{34}$$

Since there are no body forces in the particle, the particle stress is divergence free $\frac{\partial \sigma_{ik}^p}{\partial x_k} = 0$. Thus, following the classic derivation from Batchelor [9], one can replace the volume integral with a surface integral $\int_{V_p}\sigma_{ij}^p\, dV = \int_{V_p}\frac{\partial}{\partial x_k}(\sigma_{ik}^p x_j)\, dV = \int_{S_p} n_k\sigma_{ik}^p x_j\, dS$, where S_p is the particle surface and n_k is the normal vector pointing into the fluid. This yields the expression for the particle extra stress

$$\left\langle \chi\sigma_{ij}^p\right\rangle = \frac{\phi}{V_p}\left(S_{ij}^p + \Pi^p\delta_{ij} + \frac{1}{2}\epsilon_{ijk}T_k^{\text{ext}}\right), \tag{35}$$

where S_{ij}^p is the particle stresslet, Π^p is the particle pressure, and T_k^{ext} is the external torque on the particle [see Eq. (14) for the expression for torque]. The definitions of the stresslet and particle pressure are below, where $f_i = \sigma_{ik}^p n_k$ is the traction on the particle surface:

$$S_{ij}^p = \frac{1}{2}\int_{S_p} (f_i x_j + f_j x_i)\, dS - \frac{1}{3}\int_{S_p} f_k x_k \delta_{ij}\, dS, \tag{36}$$

$$\Pi^p = \frac{1}{3}\int_{S_p} f_k x_k\, dS. \tag{37}$$

In our analysis, we examine a torque-free particle $T_k^{\text{ext}} = 0$ and neglect the isotropic portion of the extra stress as it is absorbed into a pressure. Thus, one only needs to compute the particle stresslet S_{ij}^p.

Since we are interested in the extra stress up to $O(\phi\text{Wi})$, we need to compute the stresslet on an individual particle up to $O(\text{Wi})$. We perform a perturbation expansion below:

$$S_{ij}^p = S_{ij}^{p,(0)} + \text{Wi} S_{ij}^{p,(1)}, \tag{38}$$

where $S_{ij}^{p,(0)}$ is the stresslet of an individual particle in a Newtonian fluid (published in Ref. [35]), and $S_{ij}^{p,(1)}$ is the non-Newtonian correction. The traditional method for obtaining $S_{ij}^{p,(1)}$ is to solve the $O(\text{Wi})$ flow equations in Eq. (18) for velocity and pressure, compute the tractions at the interface, and substitute it into the integral in Eq. (36). However, using an integral transform technique known as the reciprocal theorem [35,36], one can write the stresslet expression using quantities that only depend on the $O(1)$ solution. Details of the derivation are provided in Appendix 3, and the final expressions are shown below.

The $O(\text{Wi})$ correction to the particle stresslet satisfies the following equation:

$$S_{ij}^{p,(1)} = R_{ijk}^{SU} U_k^{p,(1)} + R_{ijk}^{S\Omega} \Omega_k^{p,(1)} + S_{ij}^{\text{poly}}, \tag{39}$$

where R_{ijk}^{SU} and $R_{ijk}^{S\Omega}$ are the resistance tensors in Stokes flow connecting stresslet (S) with translational (U) and rotational (Ω) velocities, $[U_i^{p,(1)}, \Omega_i^{p,(1)}]$ are the $O(\text{Wi})$ corrections to the translational and rotational velocities, and S_{ij}^{poly} is an additional contribution from the polymeric torque defined below:

$$S_{ij}^{\text{poly}} = \text{sym}\left[\int_{S_p} x_i \sigma_{jm}^{\text{poly},\infty} n_m dS\right] + \int_V \frac{\partial v_{kij}^{\text{strain}}}{\partial x_m} \sigma_{km}^{\text{poly},D} dV. \tag{40}$$

In the above expression, the first integral is the force dipole on the particle using the polymeric stress evaluated at $\mathbf{u}^\infty$—i.e., $\boldsymbol{\sigma}^{\text{poly},\infty} = \boldsymbol{\sigma}^{\text{poly}}(\mathbf{u}^\infty)$. The expression sym represents the symmetric, traceless portion of a tensor—i.e., $\text{sym}(A_{ij}) = \frac{1}{2}(A_{ij} + A_{ji}) - \frac{1}{3}A_{kk}\delta_{ij}$. The second integral is a volumetric integral outside of the particle. Here, v_{kij}^{strain} is the disturbance velocity field in Stokes flow in the k direction from a unit rate of strain e_{ij}, with analytical expressions given by Kim and Karrila [35]. The quantity $\boldsymbol{\sigma}^{\text{poly},D}$ is the $O(1)$ disturbance polymeric stress—i.e., $\boldsymbol{\sigma}^{\text{poly},D} = \boldsymbol{\sigma}^{\text{poly}}(\mathbf{u}^\infty + \mathbf{u}^{(0)}) - \boldsymbol{\sigma}^{\text{poly}}(\mathbf{u}^\infty)$. The disturbance fields and volumetric integral can be evaluated in the unbound domain to the level of approximation needed for the theory.

To obtain the correction to the translational and rotational velocities of the particle, one needs to solve the following system of equations:

$$\begin{bmatrix} R_{ij}^{FU} & R_{ij}^{F\Omega} \\ R_{ij}^{TU} & R_{ij}^{T\Omega} \end{bmatrix} \begin{bmatrix} U_j^{p,(1)} \\ \Omega_j^{p,(1)} \end{bmatrix} = \begin{bmatrix} F_i^{\text{poly}} \\ T_i^{\text{poly}} \end{bmatrix}. \tag{41}$$

In the above equation, the resistance tensors (R_{ij}^{FU}, $R_{ij}^{F\Omega}$, R_{ij}^{TU}, $R_{ij}^{T\Omega}$) connect the external force (F) and torque (T) to the translational (U) and rotational (Ω) velocities in Stokes flow. The right-hand side is the contribution from the polymeric stress, with expressions written below:

$$F_k^{\text{poly}} = -\int_V \frac{\partial v_{ik}^{\text{trans}}}{\partial x_j} \sigma_{ij}^{\text{poly},D} dV, \tag{42a}$$

$$T_k^{\text{poly}} = -\int_V \frac{\partial v_{ik}^{\text{rot}}}{\partial x_j} \sigma_{ij}^{\text{poly},D} dV. \tag{42b}$$

Just like for the additional contribution to the stresslet in Eq (40), the volume integrals are evaluated outside the particle and can be performed in an unbounded domain. The quantities v_{ik}^{trans} and v_{ik}^{rot} are disturbance velocity fields in Stokes flow in the i direction from unit translation and unit rotation in the k direction. Expressions for these quantities are given in Kim and Karrila [35]. The quantity $\boldsymbol{\sigma}^{\text{poly},D}$ is the $O(1)$ disturbance polymeric stress discussed earlier.

IV. NUMERICAL METHODS

This section gives an overview of the numerical methods implemented to perform homogenization. First, we obtain orientation dynamics of the particle. The center of mass $\mathbf{x}_c$ and the orientation vector $\mathbf{p}$ evolve over time according to the following differential equations:

$$\frac{d\mathbf{x}_c}{dt} = \mathbf{U}^p, \quad \frac{d\mathbf{p}}{dt} = \boldsymbol{\Omega}^p \times \mathbf{p}, \tag{43}$$

where $\mathbf{U}^p = \mathbf{U}^{p,(0)} + \text{Wi}\mathbf{U}^{p,(1)}$ and $\boldsymbol{\Omega}^p = \boldsymbol{\Omega}^{p,(0)} + \text{Wi}\boldsymbol{\Omega}^{p,(1)}$ are the translational and rotational velocities expanded up to $O(\text{Wi})$. The $O(1)$ terms are calculated from known solutions (Jeffrey orbit solution [4]), while the $O(\text{Wi})$ contributions are calculated from the reciprocal theorem in Eqs. (41) and (42).We evolve the ordinary differential equations using a stiff Runge-Kutta (8,9) scheme with variable time stepping (function ode89 in MATLAB with tolerance 1e-8).

For a given particle orientation $\mathbf{p}(t)$, we compute the extra stress $\langle \sigma_{ij}^{\text{ex}} \rangle$ by calculating the fluctuating extra stress, given by Eqs. (32) and (33), and the particle stresslet, given by Eqs. (39)–(42). We then average $\langle \sigma_{ij}^{\text{ex}} \rangle$ over an appropriate set of orientations. The orientations we consider are the orientations the particle occupies in the long-time limit ($t \to \infty$). We then compute long-time viscometric functions such as shear viscosity, extensional viscosities, and normal stress coefficients (details of which are described in Sec. VI).

When computing the rigid body motion and the extra stress, one must compute several volume and surface integrals. These integrals are evaluated as follows. First, we transform all variables in the flow coordinates to the particle coordinates using the following rotation matrix:

$$J = \begin{pmatrix} \cos\phi \sin\theta & -\sin\phi & -\cos\phi\cos\theta \\ \sin\phi\sin\theta & \cos\phi & -\sin\phi\cos\theta \\ \cos\theta & 0 & \sin\theta \end{pmatrix}^T. \tag{44}$$

We then evaluate integrals in the particle frame of reference and then transform back into the flow coordinates. In the particle frame, the position coordinates in the outside flow are given by

$$\mathbf{x} = [x, y, z] = [ra\sin\theta\cos\phi;\ rb\sin\theta\sin\phi;\ rc\cos\theta], \tag{45}$$

where r is the radial distance from the center of the particle and a, b, c are the semiaxes of the particle. The integral of a function $f(r, \theta, \phi)$ over the volume outside the particle is

$$\int_{V_f} f(r,\theta,\phi) = \int_0^{2\pi}\int_0^{\pi}\int_1^{\infty} f(r,\theta,\phi)\, r^2 a\, b\, c\ \sin\theta\, dr\, d\theta\, d\phi. \tag{46}$$

TABLE II. Mesh sizes for volume integrals.

Particle	Aspect ratio	Mesh size $N_r \times N_\theta \times N_\phi$
Prolate	3	$35 \times 25 \times 75$
Prolate	5	$40 \times 30 \times 80$
Prolate	6	$50 \times 40 \times 90$
Oblate	3	$30 \times 20 \times 70$
Oblate	5	$40 \times 30 \times 80$
Oblate	6	$50 \times 40 \times 90$

Similarly, the surface integral of the function $f(\theta, \phi)$ over the particle is

$$\int_{S_p} f(\theta, \phi)\, dS = \int_0^{2\pi} \int_0^{\pi} f(\theta, \phi)\, g(\theta, \phi)\, \sin\theta\, d\theta\, d\phi, \tag{47a}$$

$$g(\theta, \phi) = \sqrt{b^2 c^2 \sin^2\theta \cos^2\phi + a^2 c^2 \sin^2\theta \sin^2\phi + a^2 b^2 \cos^2\theta}. \tag{47b}$$

These integrals are evaluated using Gaussian quadrature. Using the following transformations

$$\eta = \frac{2}{r} - 1, \quad u = \cos\theta, \quad v = \frac{\phi}{\pi} - 1, \tag{48}$$

the integrals are approximated via the quadrature summations

$$\int_0^{2\pi} \int_0^{\pi} f(\theta, \phi) \sin\theta d\theta d\phi = \pi \int_{-1}^{1} \int_{-1}^{1} f(u, v)\, du\, dv \approx \pi \sum_{i=1}^{N_\phi} \sum_{j=1}^{N_\theta} f(u_j, v_i) w_j^u w_i^v, \tag{49}$$

$$\int_1^{\infty} f(r) r^2 dr = 8 \int_{-1}^{1} f(\eta)\, (\eta + 1)^{-4}\, d\eta \approx 8 \sum_{k=1}^{N_r} f(\eta_k)(\eta_k + 1)^{-4} w_k^\eta, \tag{50}$$

where N_r, N_θ, N_ϕ are the number of quadrature points in the r, θ, ϕ directions and w_η, w_u, w_v are the corresponding weights for Gaussian quadrature. The number of quadrature points used in all integrals for inspecting orientation dynamics for aspect ratio $A_R = 3$ particles are $N_r = 15, N_\theta = 10, N_\phi = 35$. Evaluation of the polymeric stresslet requires finer mesh sizes with growing aspect ratios. Hence, for average stress calculations, we have used mesh sizes as provided in Table II. We have performed convergence studies to show that results are insensitive to larger number of quadrature points and have presented results for the finest mesh size tested. For aspect ratios >6, we found that sharpness of edges at the poles create large velocity gradients resulting in problems with convergence of volume integrals.

V. RESULTS—ORIENTATION DYNAMICS IN VISCOELASTIC FLUID

Before we discuss the results of the extra stress, we will discuss the orientation dynamics of spheroids in weakly viscoelastic fluids and compare against known results in Newtonian fluids.

A. Newtonian fluid

In a Newtonian fluid, the orientation dynamics of a spheroidal particle satisfies Jeffery's equation [4]:

$$\frac{d\mathbf{p}}{dt} = \langle \mathbf{\Omega} \rangle \times \mathbf{p} + \Lambda(\mathbf{I} - \mathbf{pp}) \cdot \langle \mathbf{E} \rangle \cdot \mathbf{p}, \tag{51}$$

where $\mathbf{p}$ is the orientation vector, $\langle\boldsymbol{\Omega}\rangle$ is the rate of rotation vector, and $\langle\mathbf{E}\rangle$ is the rate of strain tensor. The quantity $\Lambda = \frac{a^2-b^2}{a^2+b^2}$ is a function of the semiaxes a and b, taking the values $\Lambda = 0$ for a sphere, $0 < \Lambda < 1$ for prolate particles, and $-1 < \Lambda < 0$ for oblate particles.

In a shear flow [see Eq. (2)], the orientation vector $\mathbf{p}$ follows a periodic solution known as a Jeffery orbit. If one writes $\mathbf{p} = [\sin\theta\cos\phi, \sin\theta\sin\phi, \cos\theta]$ using the angles (θ, ϕ) illustrated in Fig 3, one gets the following solution:

$$\tan\phi = -\sqrt{\frac{1-\Lambda}{1+\Lambda}}\tan\left[\frac{1}{2}\dot{\gamma}_c\sqrt{1-\Lambda^2}(t-t_0)\right], \quad \tan\theta = \frac{\sqrt{1-\Lambda}\tan\theta_0}{\sqrt{1-\Lambda\cos(2\phi)}}, \tag{52}$$

where the initial condition is $\phi = 0$, $\theta = \theta_0$ at time $t = t_0$. The particle traces different orbits depending on the initial condition. The time period of the orbits is $T = \frac{4\pi}{\sqrt{1-\Lambda^2}}\dot{\gamma}_c^{-1} = 2\pi(A_R + A_R^{-1})\dot{\gamma}_c^{-1}$, which increases linearly with aspect ratio A_R for $A_R \gg 1$.

In pure extensional flows (i.e., $\langle\boldsymbol{\Omega}\rangle = 0$), the particle orientation evolves to a steady solution. Technically, several steady solutions are possible, each corresponding to the eigenvectors of $\langle\mathbf{E}\rangle$. However, only certain eigenvectors are stable equilibria. In general, the stable orientation that is observed is the direction corresponding to the largest eigenvalue of $\Lambda\langle\mathbf{E}\rangle$. This orientation is the direction that minimizes the particle length along the compressional axes. Thus, for a planar extensional flow in Eq. (3), the long-time orientation is

$$\text{Planar extension} \quad \mathbf{p}(t\to\infty) = \begin{cases} \hat{\mathbf{x}} & \text{(prolate)} \\ \hat{\mathbf{y}} & \text{(oblate)} \end{cases}. \tag{53}$$

In terms of the angles (θ, ϕ), these orientations are

$$\phi = \begin{cases} 0^\circ & \text{(prolate)} \\ 90^\circ & \text{(oblate)} \end{cases}, \quad \theta = \begin{cases} 90^\circ & \text{(prolate)} \\ 90^\circ & \text{(oblate)} \end{cases}. \tag{54}$$

In a uniaxial extensional flow in Eq. (4), the stable eigenvector for $\Lambda\langle\mathbf{E}\rangle$ is the extension direction $\hat{\mathbf{x}}$ for prolate particles and any vector lying in the y-z compressional plane for oblate particles. Thus, there are many different long-time orientations for oblate particles. It turns out the final orientation is the initial orientation $\mathbf{p}_0$ projected onto the y-z plane and normalized. In summary, the long-time, stable orientations are

$$\text{Uniaxial extension} \quad \mathbf{p}(t\to\infty) = \begin{cases} \hat{\mathbf{x}} & \text{(prolate)} \\ \frac{\mathbf{p}_0\cdot(\mathbf{I}-\hat{\mathbf{x}}\hat{\mathbf{x}})}{\sqrt{\mathbf{p}_0\cdot(\mathbf{I}-\hat{\mathbf{x}}\hat{\mathbf{x}})\cdot\mathbf{p}_0}} & \text{(oblate)} \end{cases}. \tag{55}$$

In terms of angles (θ, ϕ), these correspond to

$$\phi = \begin{cases} 0^\circ & \text{(prolate)} \\ 90^\circ & \text{(oblate)} \end{cases}, \quad \cos\theta = \begin{cases} 0 & \text{(prolate)} \\ \frac{\cos\theta_0}{\sqrt{\sin^2\theta_0\sin^2\phi_0+\cos^2\theta_0}} & \text{(oblate)} \end{cases}. \tag{56}$$

B. Viscoelastic fluid

When a spheroid is in a weakly viscoelastic fluid (Wi $\ll 1$), Jeffries Eq. (51) will contain a $O(\text{Wi})$ correction. This correction significantly modifies the orientation dynamics in a shear flow but does not appreciably modify the behavior in pure extensional flows.

Figures 4 and 5 show the motion of prolate and oblate particles in a shear flow. In a Newtonian fluid, the spheroids undergo Jeffery orbit motion—i.e., periodic tumbling whose path depends on the initial orientation. However, when weak viscoelasticity is present, prolate particles drift slowly to a steady alignment along the vorticity direction (i.e., $\hat{\mathbf{z}}$ or $\theta = 0^\circ$), known as log-rolling in the literature [20]. The timescale of this drift is slow—on the order of $t \sim O(\text{Wi}^{-1})$. For oblate particles, the viscoelasticity causes all particles—regardless of initial orientation—to drift into the flow-shear

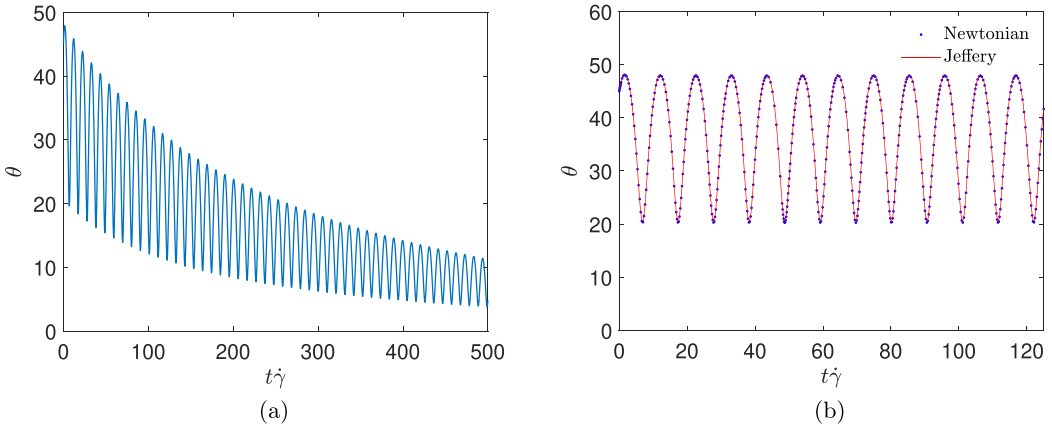

FIG. 4. Evolution of polar angle θ with dimensionless time $t\dot{\gamma}$ for a prolate particle in a shear flow with $A_R = 3$ in (a) viscoelastic fluid with $\mathrm{Wi} = 0.125$ showing eventual alignment in the vorticity direction and (b) Newtonian fluid ($\mathrm{Wi} = 0$) depicting periodic tumbling representing the Jeffery Orbit motion [4].

gradient plane (i.e., x-y plane or $\theta = 90^\circ$) and tumble periodically. The drift for this case also occurs over a slow timescale $t \sim O(\mathrm{Wi}^{-1})$. D'avino *et al.* [37] numerically studied the orientation dynamics of prolate spheroids in shear flow suspended in Giesekus and the Phan-Thien-Tanner fluids, respectively. At low Deborah numbers (De), these models behave like a second-order fluid. In the low De limit, they show that a prolate spheroid with aspect ratio $A_R = 4$ settles in a log-rolling motion, which supports our theory.

When particles are in a pure extensional flow (planar or uniaxial), the particles in a viscoelastic fluid drift to the same steady orientation as the Newtonian case. Viscoelasticity slows the dynamics toward a steady state for prolate spheroids but hastens the dynamics for oblate spheroids. Figures 6 and 7 show examples of prolate and oblate particles in a planar extensional flow, with other examples (uniaxial extensional flow) shown in Appendix 4.

Figures 8 and 9 summarize the long-time orientation behavior of prolate and oblate spheroids in viscoelastic fluids. We will examine the effective stress of a suspension of these particles in this long-time limit.

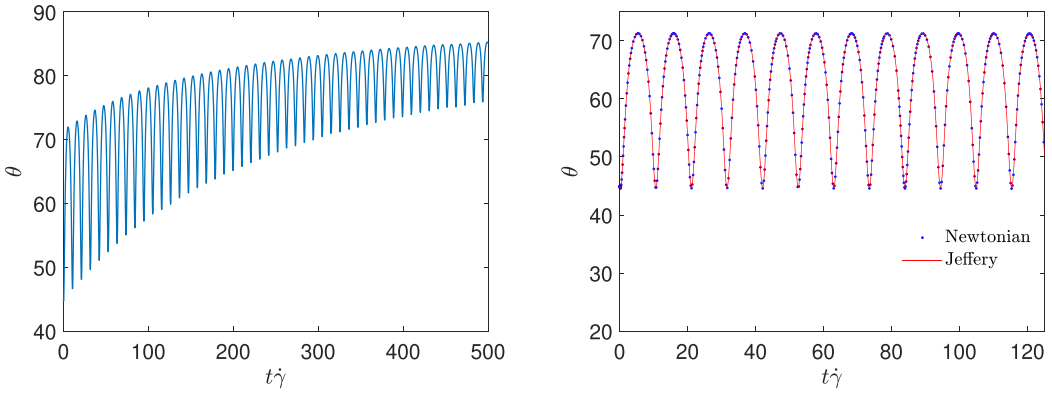

FIG. 5. Evolution of polar angle θ with dimensionless time $t\dot{\gamma}$ for an oblate particle in a shear flow with $A_R = 3$ in (a) viscoelastic fluid with $\mathrm{Wi} = 0.125$ showing eventual end-to-end tumbling in the flow-shear plane and (b) Newtonian fluid ($\mathrm{Wi} = 0$) depicting periodic tumbling representing the Jeffery Orbit motion [4].

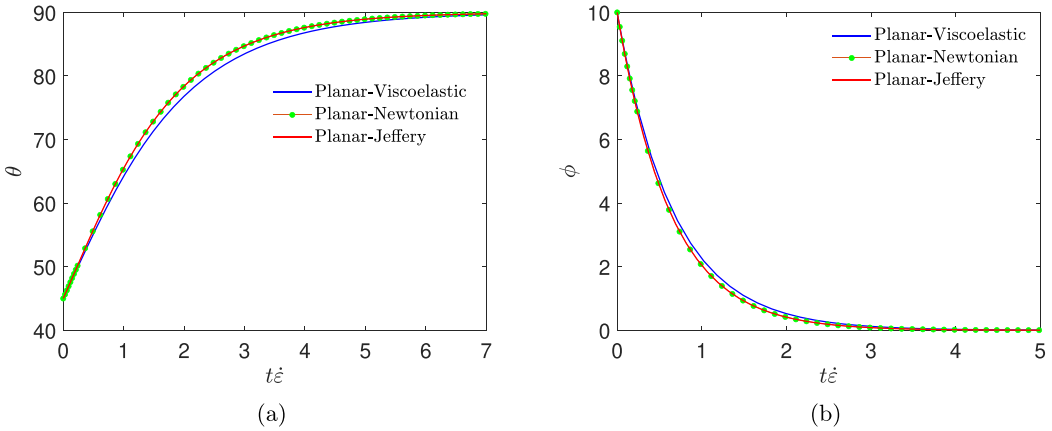

FIG. 6. Evolution of (a) polar angle θ and (b) azimuthal angle ϕ with dimensionless time $t\dot{\epsilon}$ for a prolate particle in a planar extensional flow with $A_R = 3$ and $\mathrm{Wi} = 0.1$, portraying alignment in the extension (x) direction. Newtonian dynamics ($\mathrm{Wi} = 0$) are validated using Jeffery's results [4].

VI. RESULTS—EFFECTIVE RHEOLOGICAL PROPERTIES

In this section, we discuss the rheological properties such as the effective viscosities and the effective first and second normal stress coefficients of the suspension. We will present results evaluated at the long-time orientations of the particle discussed in Sec. V.

A. Uniaxial extensional flow

In a uniaxial extensional flow [Eq. (4)], the extensional viscosity is defined as

$$\eta_{\mathrm{eff}} = \frac{\sigma_{xx} - \frac{1}{2}(\sigma_{yy} + \sigma_{zz})}{\dot{\epsilon}}, \tag{57}$$

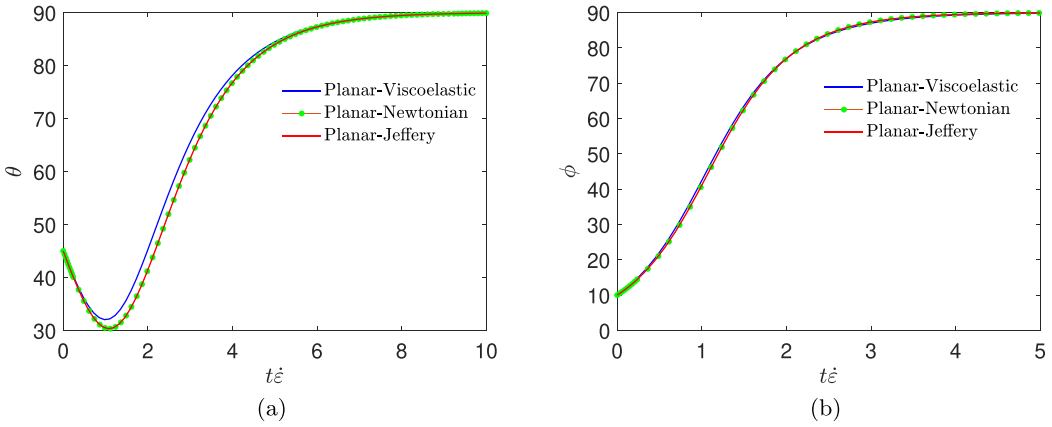

FIG. 7. Evolution of (a) polar angle θ and (b) azimuthal angle ϕ with dimensionless time $t\dot{\epsilon}$ for an oblate particle in a planar extension flow with $A_R = 3$ and $\mathrm{Wi} = 0.1$, portraying alignment in compression (y) direction. Newtonian dynamics ($\mathrm{Wi} = 0$) are validated using Jeffery's results [4].

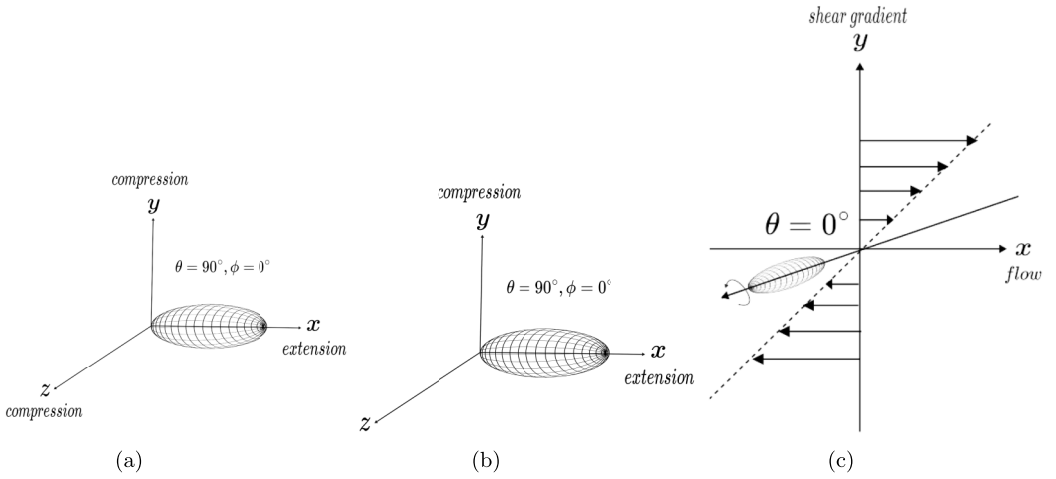

FIG. 8. Long-time orientations of a prolate particle with $A_R = 3$ suspended in a viscoelastic fluid with viscoelastic ratio $\frac{\psi_2}{\psi_1} = -\frac{1}{6}$ in (a) uniaxial extensional flow at $\mathrm{Wi} = 0.1$, exhibiting alignment in the extension direction, (b) planar extensional flow at $\mathrm{Wi} = 0.1$, showing alignment in the extension direction, and (c) shear flow at $\mathrm{Wi} = 0.125$, undergoing log-rolling in the vorticity direction.

where $\sigma_{xx}, \sigma_{yy}, \sigma_{zz}$ are the diagonal components of the total average stress and $\dot{\gamma}_c = \dot{\epsilon}$ is the elongation rate. The effective viscosity can also be written as

$$\eta_{\text{eff}} = \eta^* + 3k\mu\phi, \tag{58}$$

where $\eta^* = 3\mu[1 + \mathrm{Wi}(1 + 2\alpha)]$ is the effective viscosity of the polymeric fluid in the absence of particles and k is the dimensionless factor by which the effective viscosity is enhanced due to the particles. In a Newtonian fluid ($\mathrm{Wi} = 0$), the value of k has been reported for spheroids [9]. When the fluid is viscoelastic ($\mathrm{Wi} \neq 0$), results have been reported only for spheres [26,27]. For spheres, $k = 2.5 + \frac{75}{28}\mathrm{Wi}(1 + 2\alpha)$. In this section, we report variation of the enhancement factor k with the Weissenberg (Wi) number and particle aspect ratio.

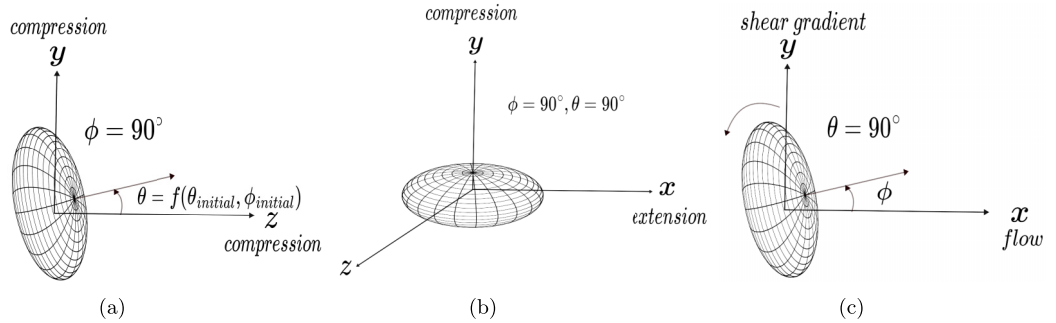

FIG. 9. Long-time orientations of an oblate particle with $A_R = 3$ suspended in a viscoelastic fluid with viscoelastic ratio $\frac{\psi_2}{\psi_1} = -\frac{1}{6}$ in (a) uniaxial extensional flow at $\mathrm{Wi} = 0.1$, exhibiting alignment in the compression (y-z) plane, (b) planar extensional flow at $\mathrm{Wi} = 0.1$, showing alignment in the compression (y) direction, and (c) shear flow at $\mathrm{Wi} = 0.125$, undergoing end-to-end tumbling in the flow-flow gradient plane (i.e., x-y plane).

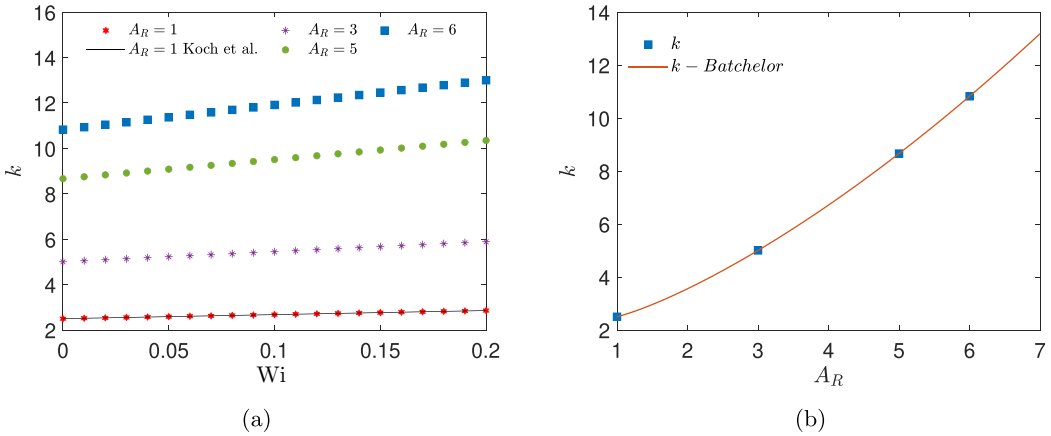

FIG. 10. Enhancement factor k for extensional viscosity of prolate particles in a uniaxial extensional flow at their long-time orientation ($\mathbf{p} = \hat{\mathbf{x}}$). (a) Viscoelastic fluid with $\alpha = \frac{\psi_2}{\psi_1} = -\frac{1}{6}$ for different Weissenberg numbers Wi and particle aspect ratios A_R. Results are also plotted for spheres as reported by Koch and Subramanian [26]. (b) The results for different aspect ratios in a Newtonian fluid (Wi = 0) are validated by comparison with the benchmark study of Batchelor [9].

1. Prolate spheroid

In Fig. 10, the enhancement factor k increases with an increase in Weissenberg number Wi for all aspect ratios of the prolate particle. This implies that as viscoelasticity or elongation rate increases, the $O(\phi)$ contribution to effective viscosity also increases. This can be attributed to two reasons. First, increasing Wi increases polymer stretching in the disturbance velocity field, increasing the fluctuating polymer stress. It also increases the stress on the particle, increasing the particle stresslet. We also note that, for the same Wi, the effective viscosity is higher for the particle with a higher aspect ratio A_R. When the particle is pointing in the extension direction, its length along this direction increases for an increase in aspect ratio. This results in an increase in force dipole on the particle, and as a result, the stresslet increases, which in turn increases the effective viscosity. Figure 10(a) shows that our results match the results for spheres in viscoelastic fluids found by Koch and Subramanian [26], while Fig. 10(b) shows that the results quantitatively match the results for spheroids in a Newtonian fluid [9].

2. Oblate spheroid

When one applies uniaxial extensional flow to a suspension of randomly oriented oblate spheroids, the final orientation of the particles can take many angles [see Eqs. (55) and (56)]. Thus, one must perform ensemble averaging over all these possible directions to obtain the long-time extensional viscosity. Thus, for an initial orientation $\mathbf{p}_0$, we calculate the final orientation $\mathbf{p}_f$ in Eq. (56) and compute the extensional viscosity at this angle $\eta_{\text{eff}}(\mathbf{p}_f|\mathbf{p}_0)$. We then average over all initial angles to get the ensemble average of η_{eff}:

$$\langle \eta_{\text{eff}} \rangle = \int \eta_{\text{eff}}(\mathbf{p}_f|\mathbf{p}_0) p(\mathbf{p}_0) d\mathbf{p}_0. \tag{59}$$

We assume the initial probability distribution is random—i.e., $p(\mathbf{p}_0)d\mathbf{p}_0 = \frac{1}{4\pi}\sin\theta d\theta d\phi$. The integral above is computed using the Gaussian quadrature. After this procedure is performed, we obtain the correction factor k as described in Eq. (58).

Figure 11 shows the trend of the enhancement factor k for different aspect ratios and Wi. The average enhancement factor k increases with the Weissenberg number Wi for all aspect ratios of the oblate particle, following the same physical arguments as before. Akin to the prolate case, for

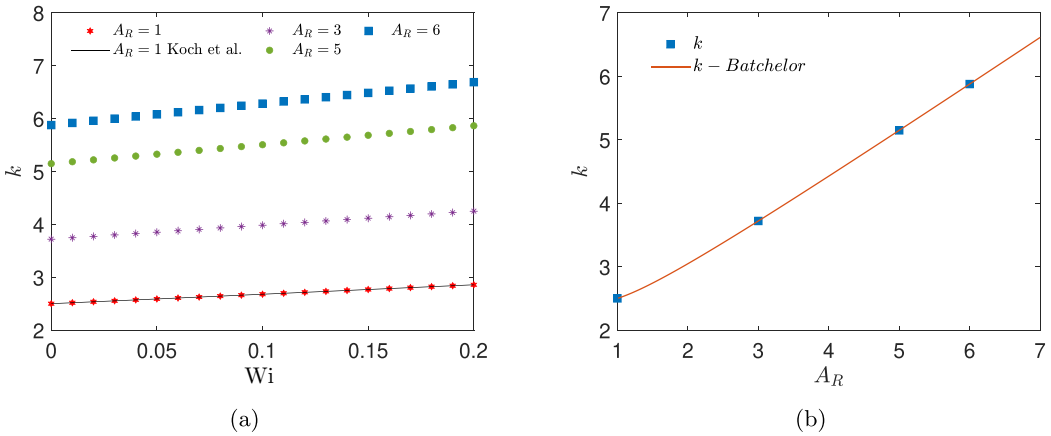

FIG. 11. Enhancement factor k for extensional viscosity of oblate particles in a uniaxial extensional flow, starting from an initial random distribution of orientations and averaging over all final orientations (a) Viscoelastic fluid with $\alpha = \frac{\psi_2}{\psi_1} = -\frac{1}{6}$ for different Weissenberg numbers Wi and particle aspect ratios A_R. Results are also plotted for spheres as reported by Koch and Subramanian [26]. (b) The results for different aspect ratios in a Newtonian fluid (Wi = 0) are validated by comparison with the benchmark study of Batchelor [9].

the same Wi, the effective viscosity is higher for the particle with a higher aspect ratio A_R. Figures 11(a) and 11(b) also include benchmarks for spherical particles in a viscoelastic fluid [26] and spheroidal particles in a Newtonian fluid [9].

B. Planar extensional flow

For planar extensional flow [Eq. (3)], there are two effective viscosities defined as

$$\eta_{1,\text{eff}} = \frac{\sigma_{xx} - \sigma_{yy}}{\dot{\epsilon}}, \tag{60a}$$

$$\eta_{2,\text{eff}} = \frac{\sigma_{zz} - \sigma_{yy}}{\dot{\epsilon}}, \tag{60b}$$

where $\sigma_{xx}, \sigma_{yy}, \sigma_{zz}$ are the diagonal components of the total average stress and $\dot{\gamma}_c = \dot{\epsilon}$ is the elongation rate. The first and second planar effective viscosities can also be written as

$$\eta_{1,\text{eff}} = \eta_1^* + 4k_1\mu\phi, \tag{61a}$$

$$\eta_{2,\text{eff}} = \eta_2^* + 2k_2\mu\phi, \tag{61b}$$

where $\eta_1^* = 4\mu$ and $\eta_2^* = 2\mu[1 - 2\text{Wi}(1 + 2\alpha)]$ are extensional viscosities in the absence of particles, and k_1 and k_2 are dimensionless contributions from the particles. As stated before, results have been previously reported for spheroids in Newtonian fluids (Wi = 0) and spheres in weakly viscoelastic fluids (Wi $\neq$ 0) [9,26,27]. For a sphere, $k_1 = 2.5$ and $k_2 = 2.5 - \frac{75}{14}\text{Wi}(1 + 2\alpha)$. This section studies the variation of k_1 and k_2 with Weissenberg number Wi for nonspherical particles. We will examine results in the long-time limit [i.e., $\mathbf{p} = \hat{\mathbf{x}}$ for prolate particles and $\mathbf{p} = \hat{\mathbf{y}}$ for oblate particles, see Eqs. (53) and (54)].

1. Prolate spheroid

In Fig. 12(a), k_1 increases with both Wi and aspect ratio A_R for a prolate particle. The system experiences an increase in the first planar effective viscosity due to stretching of polymers in the fluid phase as the shear rate/viscoelasticity increases as well as an increase in length (i.e., force

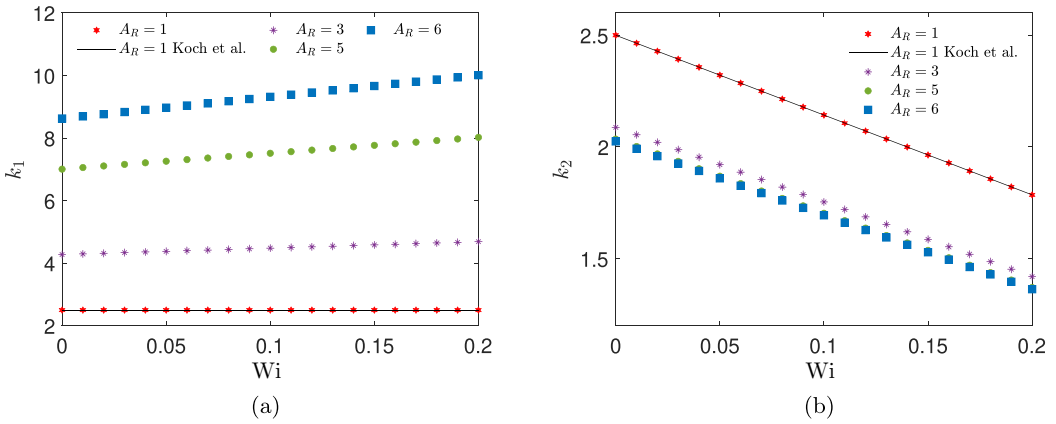

FIG. 12. (a) Enhancement factor k_1 for first planar viscosity and (b) enhancement factor k_2 for second planar viscosity for prolate particles with different aspect ratios A_R and Weissenberg numbers Wi at their long-time orientation ($\mathbf{p} = \hat{\mathbf{x}}$). The normal stress ratio is $\alpha = \frac{\psi_2}{\psi_1} = -\frac{1}{6}$. The results for spheres ($A_R = 1$) are validated by comparison with the benchmark study of Koch and Subramanian [26].

dipole) along the extension direction with an increase in aspect ratio. Thus, the resistance to the flow in the flow-compression (x-y) plane increases with Wi and A_R. In Fig. 12(b), the second planar effective viscosity decreases with Wi and A_R.

Figure 13 shows the enhancements in first and second planar effective viscosities in a Newtonian fluid for various aspect ratios validated by comparison with the benchmark study of Batchelor [9].

2. Oblate spheroid

In a planar extensional flow, an oblate particle orients its shortest axis along the compression direction (y direction) and has its two longest axes lying in the x-z plane. In this state [Fig. 14(a)], k_1 increases with both Wi and aspect ratio A_R, for similar reasons discussed above. In Fig. 14(b), the second planar effective viscosity decreases with Wi but, unlike the prolate case, has a nonmonotonic

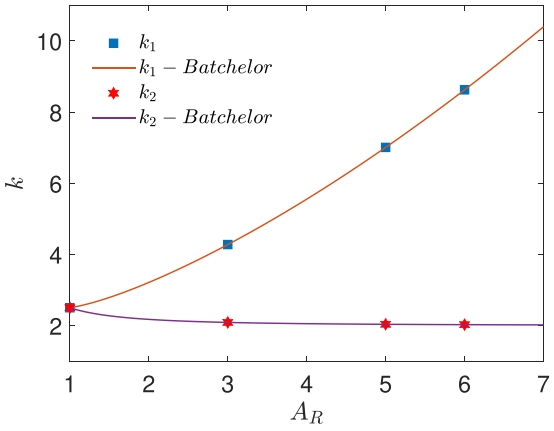

FIG. 13. Enhancement factors k_1 and k_2 for the first and second planar viscosities for a prolate particle with different aspect ratios A_R at its long-time orientation ($\mathbf{p} = \hat{\mathbf{x}}$) in a Newtonian fluid (Wi = 0). The results are validated by comparison with the benchmark study of Batchelor [9].

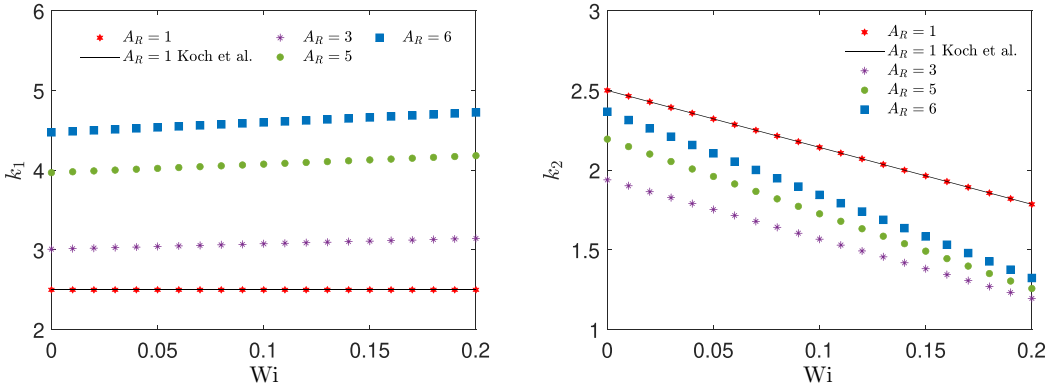

FIG. 14. (a) Enhancement factor k_1 for first planar viscosity and (b) enhancement factor k_2 for second planar viscosity for oblate particles with different aspect ratios A_R and Weissenberg numbers Wi at their long-time orientation ($\mathbf{p} = \hat{\mathbf{y}}$). The normal stress ratio is $\alpha = \frac{\psi_2}{\psi_1} = -\frac{1}{6}$. The results for spheres ($A_R = 1$) are validated by comparison with the benchmark study of Koch and Subramanian [26].

dependence on the aspect ratio A_R. Figure 15 benchmarks the code against known results for a Newtonian fluid.

C. Shear flow

In a shear flow [Eq. (2)], the viscometric functions are the shear viscosity

$$\eta_{\text{eff}} = \frac{\sigma_{xy}}{\dot{\gamma}} \tag{62}$$

and the first and second normal stress coefficients

$$\psi_{1,\text{eff}} = \frac{\sigma_{xx} - \sigma_{yy}}{\dot{\gamma}^2}, \tag{63a}$$

$$\psi_{2,\text{eff}} = \frac{\sigma_{yy} - \sigma_{zz}}{\dot{\gamma}^2}, \tag{63b}$$

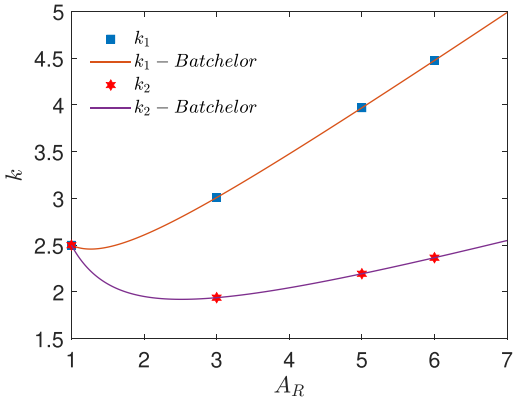

FIG. 15. Enhancement factors k_1 and k_2 for the first and second planar viscosities for an oblate particle with different aspect ratios A_R at its long-time orientation ($\mathbf{p} = \hat{\mathbf{y}}$) in a Newtonian fluid (Wi = 0). The results are validated by comparison with the benchmark study of Batchelor [9].

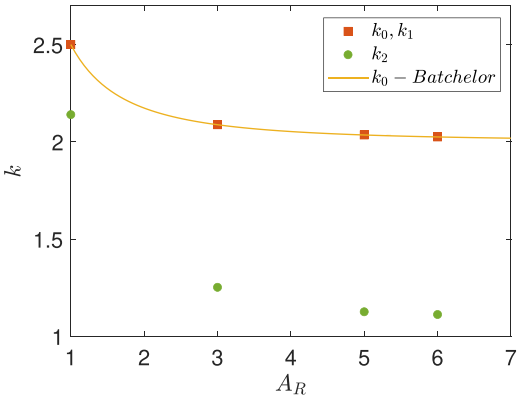

FIG. 16. Enhancement in effective shear viscosity and first and second normal stress coefficients for a prolate particle in a second-order fluid at its long-time orientation ($\mathbf{p} = \hat{\mathbf{z}}$). The normal stress ratio is $\frac{\psi_2}{\psi_1} = -\frac{1}{6}$. At this orientation, $k_0 = k_1$.

where σ_{xx}, σ_{yy}, and σ_{xy} are the components of the average stress tensor and $\dot{\gamma}_c = \dot{\gamma}$ is the shear rate. These viscometric functions can be rewritten as

$$\eta_{\text{eff}} = \mu(1 + k_0\phi), \tag{64a}$$

$$\psi_{1,\text{eff}} = \psi_1(1 + k_1\phi), \tag{64b}$$

$$\psi_{2,\text{eff}} = \psi_2(1 + k_2\phi), \tag{64c}$$

where (k_0, k_1, k_2) are contributions from the presence of particles. Author of previous studies published results for spheres in viscoelastic fluids and found that $k_0 = k_1 = \frac{5}{2}$ and $k_2 = \frac{75}{28} + \frac{5}{56}\alpha^{-1}$ up to $O(\text{Wi})$ [26,27]. Here, we will examine what occurs for nonspherical particles.

1. Prolate spheroid

We find that the viscometric functions (k_0, k_1, k_2) do not vary linearly with Wi at a given particle orientation. Since at a long time, a prolate particle aligns in one specific direction (the vorticity direction $\mathbf{p} = \hat{\mathbf{z}}$), the long-time viscometric functions do not depend on Wi up to $O(\text{Wi})$. Note, there may be a higher-order dependence on Wi, but in this paper, we cannot capture such behavior due to the applicability of the second-order fluid model. Einarsson *et al.* [27] have suggested that, at $O(\text{Wi}^2)$, the suspension shear-thickens for an Oldroyd-B fluid.

Figure 16 plots how factors k_0, k_1, and k_2 for the shear viscosity and first and second normal stress coefficients depend on the particle aspect ratio A_R. The shear viscosity and effective first and second normal stress coefficients decrease with aspect ratio. The enhancement factors for the shear viscosity and first normal stress coefficient are equal for this long-time orientation. Up to the level of approximation in our theory, the enhancement factor k_0 for shear viscosity is the same as in a Newtonian fluid (Einstein correction), with results published in many manuscripts [9,35]. We note that the contribution to the viscometric functions due to the stresslet has been numerically evaluated by D'Avino *et al.* [37] in shear flow for a prolate spheroid. They considered the Giesekus and Phan-Thien-Tanner models for their analysis. In the low Deborah number De regime, these models behave like a second-order fluid model. However, they did not account for the effects of the particle-induced fluid stress in the stress equation.

2. Oblate spheroid

At long time, an oblate particle in a shear flow tumbles in the flow-shear gradient plane. Thus, for a randomly distributed set of oblate spheroids at $t = 0$, the long-time orientations at $t \to \infty$ will

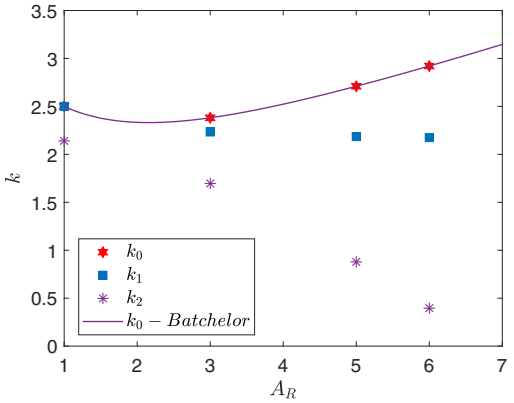

FIG. 17. Enhancement in average shear stress and first and second normal stress coefficients as a variation of aspect ratio A_R for an oblate particle in a second-order fluid with viscoelastic ratio $\frac{\psi_2}{\psi_1} = -\frac{1}{6}$ at the long-time orientation $\theta = 90^\circ$ with tumbling in a flow-shear plane averaged over $\phi \in [0, 2\pi]$.

be uniformly distributed in the flow/shear gradient plane. We thus perform an ensemble averaging over $\phi \in [0, 2\pi]$ and $\theta = \frac{\pi}{2}$. For example,

$$\langle \psi_{1,\text{eff}} \rangle = \frac{1}{2\pi} \int_0^{2\pi} \psi_{1,\text{eff}}(\phi, \theta = \pi/2)\, d\phi. \tag{65}$$

Figure 17 plots the viscometric functions. We find that the viscometric functions are independent of Wi but depend on aspect ratio A_R. To understand this observation, we can decompose the extra stress tensor $\langle \sigma_{ij}^{\text{ex}} \rangle$ as follows:

$$\left\langle \sigma_{ij}^{\text{ex}} \right\rangle = \phi \tilde{\sigma}_{ij}^{(0)} + \phi \text{Wi} \tilde{\sigma}_{ij}^{(1)}. \tag{66}$$

The enhancements in the viscometric functions are thus

$$k_0 = \tilde{\sigma}_{12}^{(0)} + \text{Wi} \tilde{\sigma}_{12}^{(1)}, \tag{67}$$

$$k_1 = \frac{1}{2\text{Wi}} \left[\tilde{\sigma}_{11}^{(0)} - \tilde{\sigma}_{22}^{(0)} \right] + \frac{1}{2} \left[(\tilde{\sigma}_{11}^{(1)} - \tilde{\sigma}_{22}^{(1)} \right], \tag{68}$$

$$k_2 = \frac{1}{2\alpha\text{Wi}} \left[\tilde{\sigma}_{11}^{(0)} - \tilde{\sigma}_{22}^{(0)} \right] + \frac{1}{2\alpha} \left[\tilde{\sigma}_{11}^{(1)} - \tilde{\sigma}_{22}^{(1)} \right]. \tag{69}$$

At a given orientation, the effective viscosity should only be an even function of shear rate, i.e., $\tilde{\sigma}_{12}^{(1)} = 0$. Thus, k_0 does not depend on Wi up to $O(\text{Wi})$. If we perform an ensemble average of $\tilde{\sigma}^{(0)}$ in the shear/shear gradient plane, one can show that this is proportional to $\langle E_{ij} \rangle$, which has no normal stress contributions. Thus, the averaged k_1 and k_2 are also independent of Wi.

VII. CONCLUSIONS

In this paper, we examined the orientation of spheroids in weakly viscoelastic fluids under three canonical flow fields: (a) shear, (b) planar extensional, and (c) uniaxial extensional flows. The long-time orientation information was then used to determine the effective stress in a dilute suspension of non-Brownian spheroids. We computed the $O(\phi)$ (i.e., Einstein) corrections to viscometric functions (e.g., shear viscosity, extensional viscosities, first and second normal stress coefficients) in the weak viscoelastic limit. The main conclusions are stated below:

(1) In a Newtonian fluid, spheroids in a shear flow undergo periodic tumbling whose path depends on the initial condition (Jeffrey orbits). In a weak viscoelastic fluid, normal stresses alter

this behavior. Prolate particles slowly settle into a log-rolling motion along the vorticity direction ($\mathbf{p} = \hat{\mathbf{z}}$), while oblate particles drift to the flow/shear gradient plane and tumble.

(2) In pure extensional flows, the orientation dynamics are not appreciably different in Newtonian and weakly viscoelastic fluids. The spheroids transition to a steady orientation, with the final orientation minimizing the length spanned in the compressional direction. Since many such orientations exist for an oblate particle in a uniaxial extensional flow, the final orientation in this case is a function of the initial orientation.

(3) The average stress in a viscoelastic fluid is a sum of two contributions: one from the force dipole on the particles (stresslet) and one from the fluctuations in velocity in the bulk fluid (fluid-induced particle stress). The latter contribution is unique to viscoelastic fluids due to the nonlinearity of the constitutive model.

(4) The viscometric functions in extensional flows exhibit the following trends. In a uniaxial extensional flow, the effective viscosity is enhanced by the presence of the particle by a factor which increases with an increase in aspect ratio and Weissenberg number, suggesting that particles aid in extensional thickening. In a planar extensional flow, the $O(\phi)$ contribution to the first planar extensional viscosity increases with Wi, while the contribution to the second planar effective viscosity decreases with Wi, suggesting that particles help thicken the former quantity and thin the latter quantity.

These trends can be explained as follows. In uniaxial extensional flow, the effective viscosity increases with the Weissenberg number because increasing the elasticity in the fluid increases the bulk stresses and particle tractions, thus increasing both the fluid induced particle stress and the particle stresslet. For both a prolate and oblate particle, with an increase in aspect ratio A_R, the particle occupies a larger length along the extension direction resulting in a greater force dipole on its surface and consequently a larger stresslet. These arguments also hold for the first planar extensional viscosity. For the second planar extensional viscosity, the normal stress in the z direction is smaller than that in the y direction because of the way $\mathbf{E} \cdot \mathbf{E}$ is defined for this flow. Consequently, the $O(\phi)$ contribution to the second planar effective viscosity is negative. As viscolelasticity increases, this term becomes more negative, and hence, the second planar effective viscosity decreases with increasing Wi.

(5) In a shear flow, at long time, the prolate particles exhibit a log-rolling state, while oblate particles tumble in the shear flow plane. At these respective orientations, the effective viscosity and the effective normal stresses for both these particles have no linear dependence on the Weissenberg number up to the level of approximation studied. For a prolate particle, the shear viscosity and first and second normal stress coefficients decrease with aspect ratio. For an oblate particle, the normal stress coefficients decrease with aspect ratio; however, the $O(\phi)$ contribution to the shear viscosity exhibits a nonmonotonic trend with aspect ratio.

In this paper, we examined nonspherical particles in the limit of weak viscoelasticity (small Weissenberg numbers). In the future, there can be other avenues to explore. A natural extension would be to examine the rheology of suspensions at higher values of Wi—i.e., stronger viscoelastic fluids or stronger shear rates. This has been done previously for spheres [27] in an Oldroyd-B fluid for effective shear viscosities up to $O(\mathrm{Wi}^2)$, which helped elucidate how particles alter the shear thinning behavior in viscoelastic fluids. Another avenue to explore would be to relax the dilute solution assumption. Hydrodynamic interactions between spheres in Newtonian fluids have been studied for concentrated suspensions ($\phi \sim 0.1$) [12]. At high concentrations, $O(\phi^2)$ and higher terms become significant. Lastly, we neglected the effect of inertia in our analysis. When the Reynolds number $\mathrm{Re} \sim O(1)$, inertial forces become prominent. There are many applications where one sees inertial and normal stress effects to be comparable; one example is microfluidic devices for particle separations [38]. For example, in shear flows, normal stresses tend to orient particles to minimize their length in the shear gradient direction [39], while fluid inertia gives the opposite behavior [40]. The coupling between these two will alter the time-dependent orientation of spheroids and the resulting rheological behavior, which has yet to be explored.

ACKNOWLEDGMENTS

The authors acknowledge support from the National Science Foundation, Grant No. CBET-2341154.

APPENDIX

1. Averaging stress by evaluating volume integral in bounded vs unbounded domains

In this subsection, we show that one can evaluate the disturbance velocity field $\mathbf{u}^{(0)}$ in an unbounded domain rather than the control volume $V = \phi^{-1}V_p$ and obtain the average stress correct to $O(\phi \mathrm{Wi})$.

Let $\mathbf{u}^{(0)}$ denote the disturbance velocity solved within the finite control volume $V = \phi^{-1}V_p$ and $\mathbf{u}^D$ represent the disturbance velocity solved in an unbounded domain. The difference between these two fields is the correction velocity field $\mathbf{u}^c$:

$$\mathbf{u}^c = \mathbf{u}^{(0)} - \mathbf{u}^D, \tag{A1}$$

where the correction field is zero on the particle surface and equal to $-\mathbf{u}^D$ on the outer surface of the finite control volume, which is at radius $r = R_V = \phi^{-1/3}$. Since in the far field, $\mathbf{u}^D \sim O(r^{-2})$ due to the particle being force and torque free, $\mathbf{u}^c \sim O(R_V^{-2}) \sim O(\phi^{2/3})$ on the outer surface. Thus,

$$\mathbf{u^{(0)}} = \mathbf{u}^D + \phi^{2/3}\tilde{\mathbf{u}}^c, \tag{A2}$$

where $\tilde{\mathbf{u}}^c$ is an $O(1)$ quantity.

When evaluating the fluctuating stress and the particle stresslet, we often come across integrals that are quadratic combinations of the disturbance field. They take the form

$$I_{ikmj} = \int_{r=r_s}^{R_V} r^{-n} \frac{\partial u_i^{(0)}}{\partial x_k} \frac{\partial u_m^{(0)}}{\partial x_j} dV, \tag{A3}$$

where $n \geqslant 0$, and the integration is from the particle surface $r = r_s$ to the radius $r = R_V$. If we substitute $\mathbf{u}^{(0)} = \mathbf{u}^D + \phi^{2/3}\tilde{\mathbf{u}}^c$, we get the following:

$$I_{ikmj} = \int_{r=r_s}^{\infty} r^{-n} \frac{\partial u_i^D}{\partial x_k} \frac{\partial u_m^D}{\partial x_j} dV + \text{correction}, \tag{A4}$$

where the correction is

$$\begin{aligned} \text{correction} = &- \int_{r=R_V}^{\infty} r^{-n} \frac{\partial u_i^D}{\partial x_k} \frac{\partial u_m^D}{\partial x_j} dV + \phi^{2/3} \int_{r=r_s}^{R_V} r^{-n} \left(\frac{\partial u_i^D}{\partial x_k} \frac{\partial \tilde{u}_m^c}{\partial x_j} + \frac{\partial \tilde{u}_i^c}{\partial x_k} \frac{\partial u_m^D}{\partial x_j} \right) dV \\ &+ \phi^{4/3} \int_{r=r_s}^{R_V} r^{-n} \left(\frac{\partial \tilde{u}_i^c}{\partial x_k} \frac{\partial \tilde{u}_m^c}{\partial x_j} \right) dV. \end{aligned} \tag{A5}$$

One can show that the first term is $O(\phi^{1+n/3})$, while the second and third terms are at most $O(\phi^{2/3})$ and $O(\phi^{4/3})$. Thus, the correction is subdominant compared with the leading term in Eq. (A4). Thus, in our derivations, we can solve the disturbance field in an unbounded domain rather than the control volume $V = \phi^{-1}V_p$ and evaluate integrals using this field over an unbounded domain as well.

2. Vanishing of $\langle u_k' \frac{E_{ij}'}{\partial x_k} \rangle$

In the derivation of the fluctuating stress, we stated that $\langle u_k' \frac{E_{ij}'}{\partial x_k} \rangle = 0$. To show this, let us first write the left-hand side as $\langle \frac{\partial}{\partial x_k}(u_k' E_{ij}') \rangle = 0$ since $\frac{\partial u_k'}{\partial x_k} = 0$. We then write this in terms of a volume

average, performing integration over a volume $V = \phi^{-1}V_p$:

$$\left\langle \frac{\partial}{\partial x_k}(u'_k E'_{ij}) \right\rangle = \frac{\phi}{V_p}\int_V \frac{\partial}{\partial x_k}(u'_k E'_{ij})dV = \frac{\phi}{V_p}\int_{S_V} u'_k E'_{ij} n_k dS. \tag{A6}$$

In the last step, we used the divergence theorem to convert the volume integral to a surface integral over the far-field surface S at radius $r = R_V = \phi^{-1/3}$. In the far field, the disturbance velocity and strain rate scale as $O(r^{-2})$ and $O(r^{-3})$, respectively, due to the particle being force and torque free. Consequently, on the surface of the control volume, they scale as $O(R_V^{-2})$ and $O(R_V^{-3})$, respectively. Thus, the above surface integral is $O(R_V^{-3}) \sim O(\phi)$, which makes the above Eq. (A6) $O(\phi^2)$ and hence unimportant in dilute solution rheology.

3. Derivation of stresslet correction using reciprocal theorem

Suppose we have two velocity fields in the same control volume V of a liquid. Both velocity fields satisfy the Stokes equations with a body force, i.e.,

$$\frac{\partial u_i}{\partial x_i} = 0, \quad \frac{\partial \sigma^N_{ij}}{\partial x_j} + b_i = 0, \tag{A7}$$

where $\sigma^N_{ij} = 2E_{ij} - -p\delta_{ij}$ is the Newtonian stress tensor, and b_i is a body force. We will add superscripts to the symbols above to demarcate the two flow fields: (β) is flow field one, while (χ) is flow field two. These flow fields are related to each other via Green's second identity, which states that

$$\int_S u_i^{(\beta)}\sigma_{ij}^{N,(\chi)} n_j^{\text{out}} dS + \int_V u_i^{(\beta)} b_i^{(\chi)} dV = \int_S u_i^{(\chi)}\sigma_{ij}^{N,(\beta)} n_j^{\text{out}} dS + \int_V u_i^{(\chi)} b_i^{(\beta)} dV. \tag{A8}$$

In the above expression, S is the surface of the control volume and n_i^{out} is the outward pointing normal vector for the control volume. Let us choose the two flow fields to be the following:

Flow 1: O(Wi) flow around the particle. Let flow one (with superscript β) be the O(Wi) flow around a spheroid in Eq. (18). Thus, we let

$$u_i^{(\beta)} = u_i^{(1)}, \tag{A9a}$$

$$\sigma_{ij}^{N,(\beta)} = \sigma_{ij}^{N,(1)}, \tag{A9b}$$

$$b_i^{(\beta)} = \frac{\partial}{\partial x_j}\left(\sigma_{ij}^{\text{poly},D}\right). \tag{A9c}$$

On the particle surface, the particle translates with the O(Wi) contribution to the rigid body motion, i.e., $u_i^{(1)} = U_i^{p,(1)} + \epsilon_{ijk}\Omega_j^{p,(1)}x_k$.

Flow 2: Stokes flow around the particle under straining motion. We will let flow two (with superscript χ) be the disturbance field around the particle in a straining flow. Here,

$$u_i^{(\chi)} = v_i, \tag{A10a}$$

$$\sigma_{ij}^{N,(\chi)} = \Sigma_{ij}, \tag{A10b}$$

$$b_i^{(\chi)} = 0, \tag{A10c}$$

where v_i and Σ_{ij} are the velocity and stress fields around the particle. On the particle surface, $v_i = V_i + \epsilon_{ijk}\omega_j x_k - e_{ij}x_j$, where x_k is the position vector from the center of mass of the particle, while V_i and ω_i are the translational and rotational speeds, and e_{ij} is the straining field. The external force and torque on the particle will be F_i^{aux} and T_i^{aux}, i.e., $F_i^{\text{aux}} = -\int_{S_p}\Sigma_{ij}n_j dS$ and $T_i^{\text{aux}} = -\int_{S_p}\epsilon_{ijk}x_j\Sigma_{km}n_m dS$, where S_p is the particle surface and n_m points into the fluid phase. These will be related to the translational and rotational speed through known resistance relationships.

We substitute the two flows into the integral expression in Eq. (A8) above. We choose the control volume V to be the volume outside of the particle. Since we are dealing with disturbance quantities, the contribution from the surface far away from the particle vanishes. We obtain

$$\int_{S_p} u_i^{(1)} \Sigma_{ij} n_j dS = \int_{S_p} v_i \sigma_{ij}^{N,(1)} n_j dS + \int_V v_i \frac{\partial}{\partial x_j} \left(\sigma_{ij}^{\text{poly},D}\right) dV, \tag{A11}$$

where S_p is particle surface and n_i is the normal vector pointing into the fluid (this is the inward pointing vector for the control volume V). Performing integration by parts on the last integral yields

$$\int_{S_p} u_i^{(1)} \Sigma_{ij} n_j dS = \int_{S_p} v_i \left(\sigma_{ij}^{N,(1)} + \sigma_{ij}^{\text{poly},D}\right) n_j dS - \int_V \frac{\partial v_i}{\partial x_j} \sigma_{ij}^{\text{poly},D} dV. \tag{A12}$$

We note that the total stress tensor at $O(\text{Wi})$ is $\sigma_{ij}^{(1)} = \sigma_{ij}^{N,(1)} + \sigma_{ij}^{\text{poly},D} + \sigma_{ij}^{\text{poly},\infty}$, where $\sigma_{ij}^{\text{poly},\infty}$ is the polymeric stress evaluated at the far-field velocity $\mathbf{u}^\infty$. Thus, the above expression becomes

$$\int_{S_p} u_i^{(1)} \Sigma_{ij} n_j dS - \int_{S_p} v_i \sigma_{ij}^{(1)} n_j dS = -\int_{S_p} v_i \sigma_{ij}^{\text{poly},\infty} n_j dS - \int_V \frac{\partial v_i}{\partial x_j} \sigma_{ij}^{\text{poly},D} dV. \tag{A13}$$

The next step in the derivation is to substitute the velocity fields on the particle surface onto the left-hand side, i.e., $u_i = U_i^{p,(1)} + \epsilon_{ijk} \Omega_j^{p,(1)} x_k$ and $v_i = V_i + \epsilon_{ijk} \omega_j x_k - e_{ij} x_j$. Substituting these expressions gives

$$-U_i^{p,(1)} F_i^{\text{aux}} - \Omega_i^{p,(1)} T_i^{\text{aux}} + S_{ij}^{p,(1)} e_{ij} = -\int_{S_p} v_i \sigma_{ij}^{\text{poly},\infty} n_j dS - \int_V \frac{\partial v_i}{\partial x_j} \sigma_{ij}^{\text{poly},D} dV. \tag{A14}$$

In obtaining the above expression, we noted that the particle is force and torque free, i.e., $F_i^{(1)} = -\int_{S_p} \sigma_{ij}^{(1)} n_j dS = 0$, $T_i^{(1)} = \int_{S_p} \epsilon_{ijk} x_j \sigma_{km}^{(1)} n_m dS = 0$.

For the last step of the derivation, we note that the auxiliary force F_i^{aux}, auxiliary torque T_i^{aux}, and the auxiliary velocity field v_i are linear in the fields (V_i, ω_i, e_{ij}). We substitute on the left-hand side of Eq. (A14) the resistance relationships for the auxiliary force and torque

$$F_i^{\text{aux}} = R_{ij}^{FU} V_j + R_{ij}^{F\Omega} \omega_j + R_{ijk}^{FE} e_{jk}, \tag{A15a}$$

$$T_i^{\text{aux}} = R_{ij}^{TU} V_j + R_{ij}^{T\Omega} \omega_j + R_{ijk}^{TE} e_{jk}. \tag{A15b}$$

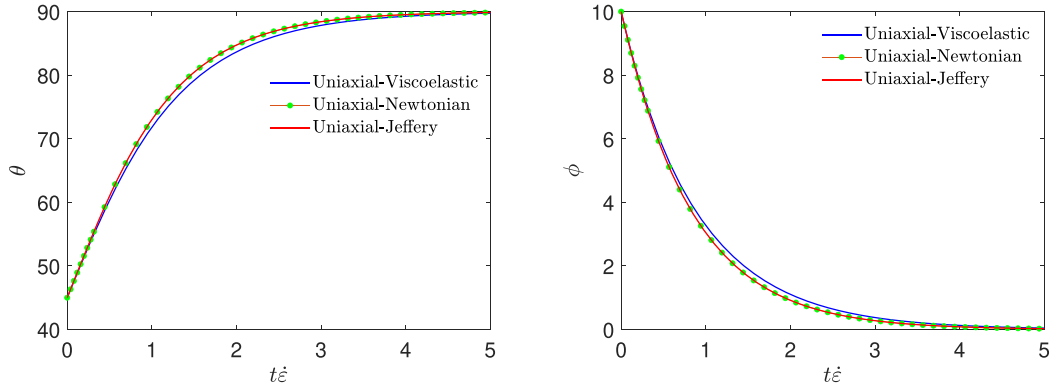

FIG. 18. Evolution of (a) polar angle θ and (b) azimuthal angle ϕ with nondimensional time $t\dot{\epsilon}$ for a prolate particle in uniaxial extensional flow with $A_R = 3$ and $\text{Wi} = 0.1$ portraying alignment in the extension direction. Newtonian dynamics ($\text{Wi} = 0$) are validated using Jeffery's results [4].

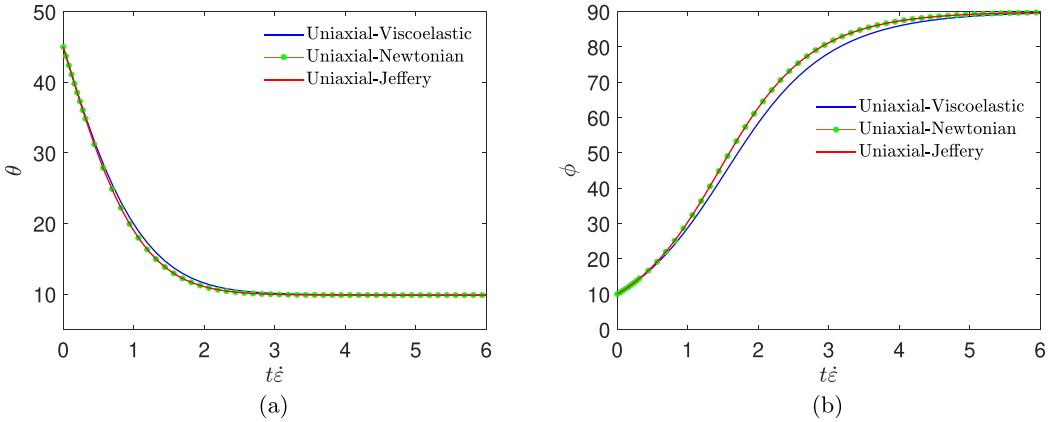

FIG. 19. Evolution of azimuthal angle ϕ with nondimensional time $t\dot{\epsilon}$ for an oblate particle in uniaxial extensional flow with $A_R = 3$ and $\mathrm{Wi} = 0.1$, portraying alignment in the compression plane. Newtonian dynamics ($\mathrm{Wi} = 0$) are validated using Jeffery's results [4].

In the above expressions, the tensors R are the resistance tensors in Stokes flow. The superscripts indicate linear relationships between forces (F), torques (T), and stresslets (S) to translation (U), rotation (Ω), and rate of strain (E). We note that these tensors follow the symmetry properties

$$R_{ij}^{FU} = R_{ji}^{FU}, \quad R_{ij}^{T\Omega} = R_{ji}^{T\Omega}, \quad R_{ij}^{F\Omega} = R_{ji}^{TU}, \quad R_{ijk}^{FE} = R_{jki}^{SU}, \quad R_{ijk}^{TE} = R_{jki}^{S\Omega}. \tag{A16}$$

On the right-hand side of Eq. (A14), we substitute that the auxiliary velocity field is

$$v_i = V_i + \epsilon_{ijk}\omega_j x_k - e_{ij}x_j, \quad \mathbf{x} \in S_p, \tag{A17a}$$

$$v_i = v_{ij}^{\mathrm{trans}} V_j + v_{ij}^{\mathrm{rot}} \omega_j + v_{ijk}^{\mathrm{strain}} e_{jk}, \quad \mathbf{x} \in V, \tag{A17b}$$

where v_{ij}^{trans}, v_{ij}^{rot}, and $v_{ijk}^{\mathrm{strain}}$ are the disturbance velocity fields in the fluid from unit translation in the j direction, unit rotation in the j direction, and unit rate of strain in the jk directions.

After performing these substitutions [i.e., substituting Eqs. (A15) and (A17) into Eq. (A14) and using the symmetry properties of the resistance tensors in Eq. (A16)], one obtains Eqs. (40)–(42). We note that $\sigma_{ij}^{\mathrm{poly},\infty}$ is force and torque free, so no surface integrals appear using this quantity in Eq. (42).

4. Results for orientation dynamics in uniaxial extension flow

Figure 18 illustrates the development of θ and ϕ for uniaxial extensional flow starting from the initial condition $\theta = 45^\circ$ and $\phi = 10^\circ$ for a prolate particle. In uniaxial extension, the prolate spheroid aligns its major axis in the extension direction (θ reaches 90°, whereas ϕ goes to 0°) at long times [see Fig. 8(a)]. This transition is slightly faster in the Newtonian fluid than the viscoelastic fluid.

Figure 19 illustrates the development of θ and ϕ for uniaxial extensional flow starting from the initial condition $\theta = 45^\circ$ and $\phi = 10^\circ$ for an oblate particle. The particle aligns its minor axis in the compression plane ($\phi = 90^\circ$). The long-time θ depends on the initial orientation of the oblate particle. Therefore, at long timescales, different particles are oriented at different θ in the compression plane [see Fig. 9(a)]. To evaluate the effective rheological properties at long-time, we will perform an ensemble average over different initial θ_i and ϕ_i as discussed in the previous sections.

[1] G. Romeo, G. D'Avino, F. Greco, P. A. Netti, and P. L. Maffettone, Viscoelastic flow-focusing in microchannels: Scaling properties of the particle radial distributions, Lab Chip **13**, 2802 (2013).
[2] C.-W. Tai and V. Narsimhan, Experimental and theoretical studies of cross-stream migration of non-spherical particles in a quadratic flow of a viscoelastic fluid, Soft Matter **18**, 4613 (2022).
[3] A. Einstein, Eine neue bestimmung der moleküldimensionen, Ann. Phys. **324**, 289 (1906).
[4] G. B. Jeffery, The motion of ellipsoidal particles immersed in a viscous fluid, Proc. R. Soc. Lond. A **102**, 161 (1922).
[5] D. Edwardes, Steady motion of a viscous liquid in which an ellipsoid is constrained to rotate about a principal axis, Quart. J. Math. **26**, 70 (1892).
[6] A. Oberbeck, Ueber stationäre Flüssigkeitsbewegungen mit Berücksichtigung der inneren Reibung, J. Reine Angew. Math. **1876**, 62 (1876).
[7] R. Roscoe, On the rheology of a suspension of viscoelastic spheres in a viscous liquid, J. Fluid Mech. **28**, 273 (1967).
[8] G. I. Taylor, The viscosity of a fluid containing small drops of another fluid, Proc. R. Soc. Lond. A **138**, 41 (1932).
[9] G. K. Batchelor, The stress system in a suspension of force-free particles, J. Fluid Mech. **41**, 545 (1970).
[10] G. K. Batchelor and J. T. Green, The determination of the bulk stress in a suspension of spherical particles to order c^2, J. Fluid Mech. **56**, 401 (1972).
[11] G. K. Batchelor and J. T. Green, The hydrodynamic interaction of two small freely-moving spheres in a linear flow field, J. Fluid Mech. **56**, 375 (1972).
[12] L. Durlofsky, J. F. Brady, and G. Bossis, Dynamic simulation of hydrodynamically interacting particles, J. Fluid Mech. **180**, 21 (1987).
[13] J. F. Brady and G. Bossis, The rheology of concentrated suspensions of spheres in simple shear flow by numerical simulation, J. Fluid Mech. **155**, 105 (1985).
[14] M. A. Jefri and A. H. Zahed, Elastic and viscous effects on particle migration in plane-Poiseuille flow, J. Rheol. **33**, 691 (1989).
[15] P. R. Nott and J. F. Brady, Pressure-driven flow of suspensions: Simulation and theory, J. Fluid Mech. **275**, 157 (1994).
[16] R. L. Powell, Rheology of suspensions of rodlike particles, J. Stat. Phys. **62**, 1073 (1991).
[17] L. G. Leal, The slow motion of slender rod-like particles in a second-order fluid, J. Fluid Mech. **69**, 305 (1975).
[18] J. Férec, E. Bertevas, B. C. Khoo, G. Ausias, and N. Phan-Thien, Rigid fiber motion in slightly non-Newtonian viscoelastic fluids, Phys. Fluids **33**, 103320 (2021).
[19] G. D'Avino, Numerical simulations on the settling dynamics of an ellipsoidal particle in a viscoelastic fluid, J. Non-Newtonian Fluid Mech. **310**, 104947 (2022).
[20] C.-W. Tai, S. Wang, and V. Narsimhan, Cross-stream migration of non-spherical particles in a second-order fluid—Theories of particle dynamics in arbitrary quadratic flows, J. Fluid Mech. **895**, A6 (2020).
[21] S. Wang, C.-W. Tai, and V. Narsimhan, Dynamics of spheroids in an unbound quadratic flow of a general second-order fluid, Phys. Fluids **32**, 113106 (2020).
[22] C.-W. Tai, A. Ahmadzadegan, A. Ardekani, and V. Narsimhan, A forward reconstruction, holographic method to overcome the lens effect during 3D detection of semi-transparent, non-spherical particles, Soft Matter **19**, 115 (2022).
[23] R. B. Bird, R. C. Armstrong, and O. Hassager, *Dynamics of Polymeric Liquids. Vol. 1: Fluid Mechanics* (John Wiley and Sons Inc., New York, 1987).
[24] A. Morozov and S. E. Spagnolie, *Introduction to Complex Fluids* (Springer, New York, 2015), pp. 3–52.
[25] P. Brunn, The motion of rigid particles in viscoelastic fluids, J. Non-Newtonian Fluid Mech. **7**, 271 (1980).
[26] D. L. Koch and G. Subramanian, The stress in a dilute suspension of spheres suspended in a second-order fluid subject to a linear velocity field, J. Non-Newtonian Fluid Mech. **138**, 87 (2006).
[27] J. Einarsson, M. Yang, and E. S. G. Shaqfeh, Einstein viscosity with fluid elasticity, Phys. Rev. Fluids **3**, 013301 (2018).
[28] B. S. Neo and E. S. G. Shaqfeh, Stresslet in a dilute suspension of rigid spheres in an Oldroyd-B fluid, Phys. Rev. Fluids **9**, 033301 (2024).

[29] P. Brunn, The motion of a slightly deformed sphere in a viscoelastic fluid, Rheol. Acta **18**, 229 (1979).
[30] A. Choudhary, S. Nambiar, and H. Stark, Orientational dynamics and rheology of active suspensions in weakly viscoelastic flows, Commun. Phys. **6**, 163 (2023).
[31] A. Langella, G. Franzino, P. L. Maffettone, D. Larobina, and G. D'Avino, Dynamics of non-spherical particles in viscoelastic fluids flowing in a microchannel, Soft Matter **19**, 9541 (2023).
[32] R. Pasquino, F. Snijkers, N. Grizzuti, and J. Vermant, The effect of particle size and migration on the formation of flow-induced structures in viscoelastic suspensions, Rheol. Acta **49**, 993 (2010).
[33] F. Del Giudice, Viscoelastic focusing of polydisperse particle suspensions in a straight circular microchannel, Microfluid. Nanofluid. **23**, 95 (2019).
[34] F. Del Giudice, G. D'Avino, F. Greco, I. De Santo, P. A. Netti, and P. L. Maffettone, Rheometry-on-a-chip: Measuring the relaxation time of a viscoelastic liquid through particle migration in microchannel flows, Lab Chip **15**, 783 (2015).
[35] S. Kim and S. Karrila, *Microhydrodynamics: Principles and Selected Applications* (Butterworth-Heinemann, Stoneham, 1991).
[36] H. Masoud and H. A. Stone, The reciprocal theorem in fluid dynamics and transport phenomena, J. Fluid Mech. **879**, P1 (2019).
[37] G. D'Avino, F. Greco, and P. L. Maffettone, Rheology of a dilute viscoelastic suspension of spheroids in unconfined shear flow, Rheol. Acta **54**, 915 (2015).
[38] J.-P. Matas, J. F. Morris, and Ã. Guazzeli, Inertial migration of rigid spherical particles in Poiseuille flow, J. Fluid Mech. **515**, 171 (1999).
[39] D. Gunes, R. Scirocco, J. Mewis, and J. Vermant, Flow-induced orientation of non-spherical particles: Effect of aspect ratio and medium rheology, J. Non-Newtonian Fluid Mech. **155**, 39 (2008).
[40] W. Mao and A. Alexeev, Motion of spheroid particles in shear flow with inertia, J. Fluid Mech. **749**, 145 (2014).